THE MACHO PROJECT LARGE MAGELLANIC CLOUD VARIABLE STAR INVENTORY. XIII. FOURIER PARAMETERS FOR THE FIRST OVERTONE RR LYRAE VARIABLES AND THE LMC DISTANCE

C. Alcock^{1,2}, D.R. Alves³, T.S. Axelrod⁴, A.C. Becker⁵, D.P. Bennett^{2,6}, C.M. Clement⁷, K.H. Cook², A.J. Drake^{2,8}, K.C. Freeman⁹, M. Geha^{2,10}, K. Griest^{2,11}, M.J. Lehner¹, S.L. Marshall², D. Minniti⁸, A. Muzzin⁷, C.A. Nelson², B.A. Peterson⁹, P. Popowski¹², P.J. Quinn¹³, A. W. Rodgers¹⁴, J.F. Rowe¹⁵, W. Sutherland¹⁶, T. Vandehei¹¹, D.L. Welch¹⁷

ABSTRACT

Shapes of RR Lyrae light curves can be described in terms of Fourier coefficients which past research has linked with physical characteristics such as luminosity, mass

 3 Columbia Astrophysics Laboratory, Columbia University, 550 West 120th Street, Mailcode 5247, New York, NY 10027

Email: alves@astro.columbia.edu

⁴Steward Observatory, University of Arizona, Tucson, AZ 85721

 $^5 \mathrm{Bell}$ Laboratories, Lucent Technologies, 600 Mountain Avenue, Murray Hill, NJ 07974

⁶Department of Physics, University of Notre Dame, Notre Dame, IN 46556

 7 Department of Astronomy & Astrophysics, University of Toronto, Toronto ON, M5S 3H8, Canada Email: cclement@astro.utoronto.ca, adam.muzzin@utoronto.ca

⁸Departmento de Astronomia, Pontifica Universidad Católica, Casilla 306, Santiago 22, Chile

 9 Research School of Astronomy and Astrophysics, Australian National University, Weston Creek, Canberra, ACT 2611, Australia

¹⁰Department of Astronomy and Astrophysics, University of California, Santa Cruz, CA 95064

¹¹Department of Physics, University of California, San Diego, 9500 Gilman Drive, La Jolla, CA 92093-0354

¹²Max-Planck-Institute for Astrophysics, Karl-Schwarschild-Str. 1, Postfach 1317, 85741 Gärching, Germany

¹³European Southern Observatory, Karl-Schwarzchild-Str. 2, 85748 Gärching, Germany

¹⁴Deceased

¹⁵Dept. of Physics & Astronomy, University of British Columbia, Vancouver BC, V6T 1Z4, Canada

 $^{16}\mbox{Department}$ of Physics, University of Oxford, Oxford OX1 3RH, U.K.

¹Department of Physics and Astronomy, University of Pennsylvania, PA 19104

²Lawrence Livermore National Laboratory, Livermore, CA 94550

¹⁷Department of Physics and Astronomy, McMaster University, Hamilton, Ontario Canada L8S 4M1

and temperature. Fourier coefficients have been derived for the V and R light curves of 785 overtone RR Lyrae variables in 16 MACHO fields near the bar of the LMC. In general, the Fourier phase differences ϕ_{21} , ϕ_{31} and ϕ_{41} increase and the amplitude ratio R_{21} decreases with increasing period. The coefficients for both the V and R magnitudes follow these patterns, but the phase differences for the R curves are on average slightly greater, and their amplitudes are about 20% smaller, than the ones for the V curves. The ϕ_{31} and R_{21} coefficients have been compared with those of the first overtone RR Lyrae variables in the Galactic globular clusters NGC 6441, M107, M5, M3, M2, ω Centauri and M68. The results indicate that many of the LMC variables have properties similar to the ones in M2, M3, M5 and the Oosterhoff type I variables in ω Cen, but they are different from the Oosterhoff type II variables in ω Cen. Equations derived from hydrodynamic pulsation models have been used to calculate the luminosity and temperature for the 330 bona fide first-overtone variables. The results indicate that they have $\log L$ in the range 1.6 to $1.8L_{\odot}$ and $\log T_{eff}$ between 3.85 and 3.87. Based on these temperatures, a mean color excess E(V-R) = 0.08 mag, equivalent to E(B-V) = 0.14 mag, has been estimated for these 330 stars. The 80 M5-like variables (selected according to their location in the ϕ_{31} – log P plot) are used to determine a LMC distance. After correcting for the effects of extinction and crowding, a mean apparent magnitude $\langle V_0 \rangle = 18.99 \pm 0.02$ (statistical) ± 0.16 (systematic) has been estimated for these 80 stars. Combining this with a mean absolute magnitude $M_V = 0.56 \pm 0.06$ for M5-like stars derived from Baade-Wesselink analyses, main sequence fitting, Fourier parameters and the trigonometric parallax of RR Lyrae, we derive an LMC distance modulus $\mu = 18.43 \pm 0.06$ (statistical) ± 0.16 (systematic) mag. The large systematic error arises from the difficulties of correcting for interstellar extinction and for crowding.

Subject headings: galaxies: distances and redshifts — Magellanic clouds — stars: variables: RR Lyrae

1. INTRODUCTION

The MACHO Project database is a valuable resource for studying the characteristics of variable stars in the LMC. In paper II of this series, Alcock et al. (1996, hereafter A96) identified 7900 RR Lyrae variables in twenty-two fields in the region of the LMC bar. The period-frequency distribution that they plotted for these variables showed that the mode was 0^d:583, indicative of an Oosterhoff (1939, 1944) type I population. In addition, there were two other peaks in the distribution, at 0^d:342 and 0^d:281, which they attributed to variables pulsating in the first and second overtone modes, respectively. The purpose of the present investigation is to perform a Fourier analysis of

the first-overtone (RR1¹⁸) RR Lyrae variables in order to determine an LMC distance. The LMC is a well known benchmark in the extragalactic distance scale, and thus new measurements of its distance are important in order to test the accuracy of standard cosmological models.

The distance to the LMC has a controversial history, and yet in recent years a standard distance modulus has emerged. This is due in part to the completion of the *Hubble Space Telescope's* key project to measure the Hubble constant with variable stars and standard candles, which employs $\mu_{LMC} = 18.5$ mag (Freedman et al. 2001). The Freedman et al. (2001) result of $H_0 = 71 \pm 10$ km s⁻¹ Mpc⁻¹ (statistical and systematic error total) is in strikingly good agreement with that derived from Wilkinson Microwave Anisotropy Probe data ($H_0 = 72 \pm 5$ km s⁻¹ Mpc⁻¹; Spergel et al. 2003). These measurements of H_0 are based on entirely different physics, and thus their agreement lends support to the accuracy of the standard LMC distance modulus adopted by Freedman et al. (2001). It is, in fact, a recent trend in the literature that most new LMC distance measurements are in excellent agreement with the standard model, and in many cases systematic errors in prior measurements are being found and corrected (e.g., Alves et al. 2002, Mitchell et al. 2002).

In this investigation, we employ the Fourier decomposition technique, a method for quantifying the structural characteristics of the observed light curves of variable stars. It was first applied to RR Lyrae variables by Simon & Teays (1982) who analysed the light curves of 70 field RR Lyrae stars. Later, Clement, Jankulak & Simon (1992) and Simon & Clement (1993, hereafter SC93) used the technique to compare the RR1 variables in six Galactic globular clusters (GGCs) with metal abundances ranging from [Fe/H]=-0.99 to -2.17 on the Zinn & West (1984, hereafter ZW) scale. In particular, they studied the Fourier phase parameter ϕ_{31} . By plotting ϕ_{31} versus log P, they discovered that the clusters were segregated according to metallicity and that, within each cluster, ϕ_{31} increases with period. To understand the physical significance of this result, SC93 analysed hydrodynamic pulsation models for first-overtone variables and found that they could derive equations for expressing both the mass and the luminosity in terms of ϕ_{31} and the pulsation period. An application of these equations to the six GGCs indicated that there was a strong correlation between mean RR1 luminosity and metal abundance of the cluster. This provided independent evidence for the existence of an RR Lyrae luminosity-metallicity relation. It also demonstrated that Fourier decomposition is a useful technique for estimating the luminosity of an RR1 variable.

Most LMC distance determinations based on RR Lyrae variables depend on the luminosity-metallicity relation. In these studies, a mean metal abundance must be adopted because spectroscopic studies by A96, Bragaglia et al. (2001) and Clementini et al. (2003, hereafter C03) have all shown that there is a range of metal abundance among the field RR Lyraes in the LMC. However, since we do not have [Fe/H] values for the individual stars in our sample, we take a different approach. In this investigation, our *modus operandi* will be to compare the Fourier parameters of the

¹⁸Throughout this paper, we adopt the system of notation that Alcock et al. (2000, hereafter A00) introduced for RR Lyrae variables: RR0 for fundamental, RR1 for first-overtone, RR2 for second-overtone pulsators, etc.

LMC RR1 variables with the ones in some well-studied GGCs. We will look for a subset of LMC RR1 variables that are similar to those in one of these clusters. Then we will assume that their RR Lyrae variables have the same mean absolute magnitude and use independent studies to determine the RR Lyrae absolute magnitudes.

2. THE OBSERVATIONAL DATA

Our investigation is based on the RR Lyrae data from 16 LMC¹⁹ fields observed for the MACHO project. The program stars were selected from a preliminary sample that included all of the (approximately 1200) RR Lyrae variables deemed to be RR1 stars according to their periods and light curve shapes. These preliminary data were instrumental magnitudes derived from the observations acquired between July 1992 and December 1995 through the MACHO B_M and R_M filters. The first step of our analysis was to derive the periods using Stellingwerf's (1978) phase dispersion minimization (PDM) technique and then to fit both the B_M and R_M magnitudes to a Fourier series of the form:

$$mag = A_0 + \sum_{j=1}^{n} A_j \cos(j\omega t + \phi_j)$$
(1)

where ω is $(2\pi/\text{period})$, t is the time of the observation and n is the order of the fit. In each case, the order of the fit was 6 and all magnitudes for which the assessed error was greater than 0.1 mag were excluded. The phase differences, $\phi_{j1} = (\phi_j - j\phi_1)$ and amplitude ratios, $R_{j1} = (A_j/A_1)$ were calculated and their standard errors were evaluated using the formulae of Petersen (1984). Since the Fourier decomposition technique is not useful for studying stars with large uncertainties in their coefficients, we included for further study only the stars with an error less than 0.3 in ϕ_{21} or an error less than 0.4 in ϕ_{31} in at least one of B or R. There were 785 stars that met these criteria. The instrumental magnitudes of these stars for the observations obtained between July 1992 and December 1999 were transformed to the Kron-Cousins V and R system using the equations derived by Alcock et al. (1999, hereafter A99). This calibration has been designated version 9903018. Calibration version numbers may also appear in some MACHO database documentation and released light curve data (e.g., Allsman & Axelrod 2001, Alcock et al. 2003).

¹⁹The LMC fields included are #2, 3, 5, 6, 10, 11, 12, 13, 14, 15, 18, 19, 47, 80, 81 and 82, all of which are close to the bar. The field of view for each field is 0.52 square degrees. An identification chart and a list of the R. A. and declination of the field centers are available at http://wwwmacho.mcmaster.ca

3. THE FOURIER ANALYSIS OF THE PROGRAM STARS

3.1. The Fourier Coefficients

The calibrated V and R magnitudes for the 785 program stars extended over a longer time base than the preliminary data and so we used the PDM technique to revise the periods before performing the Fourier analysis. Only observations obtained under good transparency conditions were included. In addition, all magnitudes for which the assessed photometric error was greater than 0.1 mag were excluded. The magnitudes were then fit to equation (1) using a 6-order fit. It turned out that the sample included 105 stars that were found to be multiperiodic²⁰ by Kovács and the MACHO collaboration (Kovács et al. 2000, A00) so that only 680 stars in the sample were monoperiodic. We present the data for these stars in Table 1. For each star, we report the results of the Fourier analysis for both the V and R magnitudes. 'N' denotes the number of observations. The quantities A_0 , A_1 , R_{j1} , ϕ_{j1} and their standard errors (σ), the amplitude and σ_{fit} were all obtained from the fit of equation (1) to the data. The coefficients for the 105 multiperiodic stars are listed in Tables 2 to 5, with the double-modes (RR01 and RR12) in Tables 2 and 3 respectively, the RR1- ν_1 stars in Table 4 and other multifrequency variables in Table 5. For the rest of this investigation, we consider only the stars listed in Table 1.

Because there is overlap between some of the LMC fields in our sample (i.e. numbers 2 and 19, 3 and 80, 5 and 10, 6 and 13, 11 and 14), there were 29 stars that were included twice in Tables 1 to 5. These stars are listed, in order of increasing right ascension, in Table 6. The table also includes the period, the mean V and R magnitudes, denoted $V >_F$ and $V >_F$, because they are the $V >_F$ and $V >_F$ and $V >_F$, because they are the $V >_F$ and $V >_F$ are the $V >_F$ and $V >_F$ and $V >_F$ and $V >_F$ are the $V >_F$ and $V >_F$ and $V >_F$ are the $V >_F$ and $V >_F$ and $V >_F$ are the $V >_F$ and $V >_F$ and $V >_F$ are the $V >_F$ and $V >_F$ and $V >_F$ are the $V >_F$ and $V >_F$ are the $V >_F$ and $V >_F$ and $V >_F$ are the $V >_F$ are the $V >_F$ and $V >_F$ are the $V >_F$ are the $V >_F$ and $V >_F$ are the $V >_F$ and $V >_F$ are the $V >_F$ are the $V >_F$ and $V >_F$ are the $V >_F$ are the

Figure 1 is a plot of $\langle V \rangle_F$ vs $[\langle V \rangle_F - \langle R \rangle_F]$ for the data listed in Table 1. For the bulk of the points, there is a general increase in $\langle V \rangle$ with increasing color, an expected consequence of reddening. The line shown in the diagram is the reddening vector which has a slope of 5.35, the relative extinction $A_V/E(V-R)$, for the Cerro Tololo V and R bandpasses (Schlegel, Finkbeiner & Davis 1998). The bright stars that appear in the upper right of the diagram are either foreground or blended stars. Their V amplitudes, mean V and R magnitudes and colors are listed in Table 7. Since blending of stars causes the amplitude of light variation to be reduced, we assume that the stars with V amplitudes less than 0.35 are probably blended, but the ones with

 $^{^{20}}$ A00 introduced a new system of subclasses to describe the frequency spectra of the multiperiodic variables: RR01 for double-mode (fundamental and first-overtone), RR12 for double-mode (first and second-overtone), RR1-PC for stars with period changes, RR1-BL for Blazhko variables and RR1- ν 1, RR1- ν 2, RR1- ν M for other multifrequency stars, where 1, 2, M indicate that there are 1, 2 or more than 2 additional frequencies.

larger amplitudes may be foreground stars. The 17 stars of Table 7 have been excluded from the rest of our investigation.

In Table 8, we list the mean magnitudes and colors for the remaining program stars in each field. The angular coordinates of the field centers (ρ and Φ) are tabulated in columns (2) and (3). Following van der Marel & Cioni (2001, hereafter vMC01), we define ρ as the angular distance between the field center and the LMC center and Φ as the position angle of the field center measured eastward from north. The origin of our adopted coordinate system is the location given by van der Marel (2001): $\alpha_0 = 5^{\rm h}29^{\rm m}$ and $\delta_0 = -69.^{\circ}5$. According to vMC01,²¹ the inclination angle of the plane of the LMC disk is $34.^{\circ}7 \pm 6.^{\circ}2$ and the line of nodes has a position angle $\Theta = 122.^{\circ}5 \pm 8.^{\circ}3$, with the near side at position angle $\Theta - 90^{\circ}$ ($\Phi \sim 30^{\circ}$) and the far side at $\Theta + 90^{\circ}$ ($\Phi \sim 210^{\circ}$). Using these values along with equation (8) of vMC01, we calculated for each field, the distance D from the observer to the point where the field center intersects the plane of the LMC disk, in terms of D_0 , the distance from the observer to the LMC center. These D/D_0 values are tabulated in column (4). In column (5), we list the average densities of the fields (number of objects per square arcmin) that were estimated by Alcock et al. (2001). In columns (6) to (8), we list the mean $\langle V \rangle_F$ and mean $\langle R \rangle_F$ magnitudes and the mean colors ($\langle V \rangle_F - \langle R \rangle_F$) along with their standard deviations. The number of program stars in each field is in column (9). The mean Vmagnitudes range from 19.24 for field #19 to 19.53 for field #15. These variations may be due to a combination of differences in distance, reddening or the intrinsic properties of the stars among the different fields. Any differences due to calibration are expected to be small. A99 found an internal precision of $\sigma_V = 0.021$, $\sigma_R = 0.019$ and $\sigma_{V-R} = 0.028$ for stars (with V < 18) in overlapping fields and it appears that this precision extends to fainter magnitudes. Among the 29 RR Lyrae variables listed in Table 6, 17 are included in both field #6 and #13. The mean $\Delta < V >_F$ for these stars is 0.012 and the mean $\Delta < R >_F$ is 0.022. Since the LMC is inclined to the plane of the sky, some of our fields must be closer than others. According to the vMC01 model, we would expect the mean magnitudes of the RR Lyrae stars in the MACHO fields that are closest to us, fields #3 and #82, to be approximately 0.06 mag brighter than the ones in the most distant fields, #10 and #13. However, this is not indicated by the data of Table 8. Differences in extinction seem to be more important. The fields with the faintest mean $\langle V \rangle$ magnitudes (#3 and #15) have mean colors that are redder than most of the other fields. If the distribution of unreddened colors of the RR Lyrae stars in these two fields is similar to the other fields, higher extinction can account for their faint mean magnitudes. We will discuss the effect of extinction in section 4. Another source of the variations may be inhomogeneities in the properties of the stars themselves. This is a problem we will address using Fourier decomposition.

In Figure 2, we plot the Fourier phase differences ϕ_{21} , ϕ_{31} and ϕ_{41} versus log P for the V data.

 $^{^{21}}$ vMC01 analysed near-infrared observations of stars at angular distances (ρ) between 2.°5 and 6.°7 from the LMC center and found a sinusoidal variation in brightness as a function of position angle. The peak to peak variation that they detected (~ 0.25 mag) was attributed to variations in the distance.

The points are plotted as open circles with three different sizes to denote different error levels: the larger the size, the smaller the error. In general, the phase differences increase with increasing period. Some of the outliers, the stars with $\phi_{31} \sim 3.5$, $\phi_{41} \sim 2.0$ and $\log P < -0.55$ are probably second overtone pulsators (RR2 variables). A96 have already pointed out that there may be second overtone pulsators among the LMC RR Lyrae population. The histograms of Figure 3 illustrate the range of errors in the Fourier phase differences. As expected, the errors in ϕ_{41} are larger than those for ϕ_{31} which in turn are larger than the errors in ϕ_{21} . This occurs because the amplitudes for the higher orders are smaller and thus it becomes increasingly difficult to derive their phases with sufficient precision. Figure 4 illustrates the relationship between the ϕ_{21} , ϕ_{31} and ϕ_{41} values for R and V. Horizontal lines are drawn at $\Delta \phi_{i1} = 0$ on each plot. Although there is a great deal of scatter, it can be noted that, in each case, the majority of the points lie above the line. The mean differences $\langle [\phi_{i1}(R) - \phi_{i1}(V)] \rangle$ are 0.03, 0.07 and 0.10 for j=2, 3 and 4 respectively, indicating that in general, the Fourier phase differences for R magnitudes are greater than the ones for V. In a comparison of ϕ_{21} and ϕ_{31} for classical Cepheids, Simon & Moffett (1985) obtained a similar result. They found that $\phi_{j1}(R) > \phi_{j1}(V) > \phi_{j1}(B)$ for j=2 and 3. They also found that the differences were greater for ϕ_{31} than for ϕ_{21} .

In Figure 5, we plot the V amplitude, the Fourier amplitude A_1 and the amplitude ratios R_{21} , R_{31} and R_{41} versus $\log P$ for the V data. The distributions of the estimated errors for R_{21} , R_{31} and R_{41} are shown in Figure 6. The error distribution is similar for all three, but since the R_{31} and R_{41} ratios are significantly lower than R_{21} , their errors are relatively large. Figure 5 illustrates that, in general, R_{21} decreases with increasing period, but there is not such a clear trend for R_{31} or R_{41} , possibly because of their larger uncertainties. Some of the short period variables with low values for A_V , A_1 and R_{21} are probably RR2 variables. Figure 7 shows the amplitude ratios (R/V) for the light curve amplitude and A_1 through A_4 . R amplitudes are generally lower than V amplitudes because pulsating stars like RR Lyrae variables have lower amplitudes when observed at longer wavelengths. In each panel, horizontal lines indicating the median are shown, and in each case, the median R/V ratio is approximately 0.8. The scatter is greater for the higher orders because their amplitudes are small and have large uncertainties. Another factor that may contribute to the scatter in the amplitude ratios is contamination. The presence of a nearby unresolved companion will reduce the observed amplitude. This is an effect we need to consider when we select a sample of stars for deriving the LMC distance.

3.2. Comparision with the RR1 Variables in Galactic Globular Clusters

For this comparison, we examine the plots of $\phi_{31} - \log P$ and $R_{21} - \log P$. We prefer ϕ_{31} to ϕ_{21} , even though $\sigma(\phi_{31}) > \sigma(\phi_{21})$ because the range in values of ϕ_{21} is very small making it difficult to detect the differences among the clusters. The $\phi_{31} - \log P$ plots are shown in Figure 8. In the upper panel, we plot $\phi_{31}(V)$ vs $\log P$ for the RR1 variables in five well-studied GGCs. The data for these clusters are taken from the following sources: NGC 6441 (Pritzl et al. 2001),

M107 (Clement & Shelton 1997), M5 (Kałużny et al. 2000, hereafter K00), M2 (Lee & Carney 1999, hereafter LC99) and M68 (Walker 1994). For NGC 6441, we have included all the variables that Pritzl et al. (2001) listed as 'RRc' but not the questionable ones (indicated as 'RRc?'). V79 was also excluded because it had a large amount of scatter on its light curve. For M5, we have included all of the variables in Table 1 of the K00 paper with the exception of V78 (considered to be an RR2 variable), V76 (classification uncertain) and V130 (large error in ϕ_{31}). Since the M5 Fourier decomposition was based on a sine series, we subtracted 3.14 from all of the published ϕ_{31} values before plotting them in Figure 8. The LC99 study of M2 did not include Fourier analysis of the variables so we analysed their published observations. Our results for the three M2 stars that we consider to be bona fide²² RR1 variables are summarized in Table 9. For M68, we excluded V5 which is probably an RR2 variable. The straight lines in the upper panel are least squares fits to the data for each cluster. In the central panel, these lines are plotted again, along with the $\phi_{31}(V)$ values for the LMC stars with $\sigma(\phi_{31}) < 0.4$. The lower panel is a repeat of the central panel, but it also includes points plotted for the RR1 variables in M3 from Kałużny et al. (1998) and ω Centauri from the Clement & Rowe (2000) study based on the observations of Kałużny et al. (1997). The $\phi_{31} - \log P$ plots for the GGCs indicate that in general, the higher the metallicity,²³ the higher the line lies in the diagram. Most of the LMC RR1 variables are distributed between the M107 and M68 lines. Many have $\phi_{31} - \log P$ values similar to the ones in M2, M3, M5 and the Oosterhoff type I (OoI) variables in ω Centauri, i.e. the ones with $\log P < -0.44$. However, not many are similar to the OoII variables in ω Cen, the ones with longer periods. There are also a significant number (with ϕ_{31} between 2.0 and 3.0) that do not have counterparts among the RR1 variables in the well-studied GGCs. These objects are worthy of further investigation.

The R_{21} – log P plots are shown in Figure 9. In the upper panel, we plot the data for the RR1 variables in M107, M5, M2 and M68. Lines based on least squares fits to the points are plotted for M5, M2 and M68. However, we do not plot a line for M107 because, although the five stars with the shortest periods show a steady decrease in R_{21} with increasing period, the other two (with log $P \sim -0.5$) do not follow the sequence. Instead, they lie among the M5 points. In the central panel, these lines are plotted again, along with the LMC variables. The lower panel is the same as the central panel, but includes points for M3 and ω Centauri. Like the previous figure, Figure 9 illustrates that some of the LMC RR1 variables have $R_{21} - \log P$ values similar to the ones in

²²LC99 presented photometry for 30 RR Lyrae variables, 12 of which they classified as type c. We include only three of these 'type c' stars in Table 9 because three of them (LC 651, 715 and 733) appear to be pulsating in the second overtone mode. Four others (V15, V18, V20 and LC 939) were excluded because their light curves have night-to-night variations similar to those of the variables in M55 that Olech et al. (1999) classified as non-radial pulsators. The stars LC 608 and 1047 were also excluded because of a large amount of scatter on their light curves. In the case of the former, it may be caused by large period changes and for the latter, it may be due to light contamination from a nearby star.

 $^{^{23}}$ The [Fe/H] values that Harris (1996) list in his 2003 catalog update for NGC 6441, M107, M5, M3, M2 and M68 are -0.53, -1.04, -1.27, -1.57, -1.62 and -2.06, respectively. The ZW values for the same six clusters are -0.59, -0.99, -1.40, -1.66, -1.62 and -2.09.

M2, M3, M5 and the OoI variables in ω Cen, but they are different from the majority of the ω Cen variables which have OoII characteristics.

Since one of the aims of our investigation is to determine the LMC distance, we want to select a group of LMC variables that have properties similar to the variables in a well-studied GGC. We will then make the assumption that these stars have a similar distribution of luminosities so that their absolute magnitudes can be derived by independent methods. We conclude that M5 is more suitable for this purpose than M2 or M3 because the M5 study by K00 includes a more complete sample (13) of RR1 variables with well-determined Fourier coefficients. In addition, there have been independent studies of the absolute magnitude of the HB stars in M5. Storm, Carney & Latham (1994) performed a Baade-Wesselink analysis on two of its RR Lyrae variables and Carretta et al. (2000) derived $M_V(HB)$ from main sequence fitting. These studies will be discussed further in section 5.3.

3.3. Luminosity, Mass and Temperature Derived from Fourier Coefficients

SC93 derived an equation, based on hydrodynamic pulsation models, for calculating the luminosity of an RR1 variable from ϕ_{31} and period:

$$\log L/L_{\odot} = 1.04 \log P - 0.058\phi_{31} + 2.41 \tag{2}$$

In an independent investigation, based on observations of 93 RR1 variables in eight different stellar systems, Kovács (1998, hereafter K98) derived an equation relating the absolute magnitude M_V of an RR1 variable to its period and Fourier coefficients ϕ_{21} and A_4 :

$$M_V = 1.261 - 0.961P - 0.044\phi_{21} - 4.447A_4. \tag{3}$$

The phase difference ϕ_{21} in the K98 equation is based on a sine series fit so we subtracted 1.57 from our ϕ_{21} values which are based on a cosine series. SC93 also used their pulsation models to derive an equation relating mass to ϕ_{31} and period:

$$\log M/M_{\odot} = 0.52 \log P - 0.11\phi_{31} + 0.39. \tag{4}$$

Combining this with the period/mean density law (equation 2 in their paper), we can derive an equation for calculating the temperature:

$$\log T_{eff} = 3.775 - 0.1452 \log P + 0.0056\phi_{31}. \tag{5}$$

Using equations (2), (3) (4) and (5) with the V data, we calculated $\log L$, M_V , $\log M$ and $\log T_{eff}$ for the 'Table 1' stars with $\sigma(\phi_{31}) < 0.4$. Since these equations are valid only for RR1 variables, we have included only stars with periods in the range $-0.56 < \log P < -0.4$ and amplitudes $A_V > 0.3$. Stars with shorter periods and lower amplitudes are probably RR2 variables and stars with longer periods have anomalous light curves indicating that they are probably not bona fide

RR1 variables. In addition, we restricted the sample to stars with amplitude ratios in the range: $0.75 < A_R/A_V < 0.85$. Amplitude ratios outside this range may occur if the phase coverage on the light curve is incomplete or if the star has a faint unresolved companion, in which case the mean magnitude and amplitude are not reliable. Also, if a variable is an eclipsing binary, its amplitude ratio should be close to unity and therefore > 0.85. A total of 330 stars met the above criteria. We will refer to these as the 'bona fide' RR1 stars. In column (2) of the electronic version of Table 1, these stars are denoted 'bf'.

Figure 10 is a plot of $\log L/L_{\odot}$ versus $\log T_{eff}$ for these 330 bona fide RR1 variables. It demonstrates that the stars in our sample have $\log L$ ranging from ~ 1.6 to $\sim 1.8 L_{\odot}$ and $\log T_{eff}$ between ~ 3.85 and ~ 3.87 , values appropriate for first-overtone pulsators on the blue side of the instability strip according to the models of Bono et al. (1997) and Yoon & Lee (2002). In Figures 11 and 12, we plot $\log L$ and M_V versus $\langle V \rangle_F$ with the results for each of the 16 fields shown in different panels. The lines in Figure 11 have a slope of -0.4. They are plotted at an arbitrary position, but are set at the same position in each panel so that any variations among the different fields can be readily recognized. The standard deviation of the fit of the hydrodynamic models to equation (2) was $\Delta \log L = 0.035$, but the scatter for the individual fields is greater than that. The situation is similar in Figure 12 where the lines are plotted with a slope of unity. The standard deviation that K98 derived for equation (3) was 0.042. Clement & Rowe (2000) made similar plots for the RR1 variables in ω Centauri and the fit was much better. If the variations in apparent magnitude among the stars in the individual LMC fields are due primarily to differences in luminosity, we should see better correlations in Figures 11 and 12. On the other hand, if the variations are due to differences in distance as well as luminosity, we would not expect to see correlations in these figures. However, a difference of 0.5 mag would require a difference of about 25% in distance which is certainly not expected a priori. We conclude that differential reddening and crowding within the individual fields must also contribute to the scatter.

In Figure 13, we plot $\log L$ vs. M_V and it is clear that these two quantities are correlated even though equations (2) and (3) were derived by independent methods. Since C03 established that there exists a luminosity-metallicity relation with slope = $\Delta M_V/\Delta \text{Fe/H} = 0.214 \pm 0.047$ among the LMC RR Lyrae variables, we assume that the brighter stars are more metal-poor than the faint ones. This means that their bolometric corrections will be different and since $\log L$ refers to the bolometric luminosity, we should take this into account when comparing $\log L$ with M_V . Bessell & Germany (1999, hereafter BG99) showed the relationship between bolometric correction (BC) and (V-R) color for four different values of [Fe/H] (Figure 8 in their paper). From a comparison of BC for [Fe/H]=-1.0 and -2.0 at $(V-R)_0 = 0.14$ mag, a typical intrinsic color for an RR1 variable, we see that $\Delta BC/\Delta [\text{Fe/H}] \sim 0.03$. Combining this with C03's slope for the luminosity-metallicity relation (0.21), we derive a slope of -0.46 for the $\log L/L_{\odot}$ vs. M_V plot. The envelope lines in the diagram are plotted with this slope and are separated by $\Delta \log L = 0.07$, twice the standard deviation in the fit of equation (2) to the models. The actual slope of the plotted points (-0.53) is steeper than -0.46. Nevertheless, 72% of the points lie between the envelope lines. In section 5.3,

we will derive a mean absolute magnitude for the M5-like variables based on Fourier coefficients.

4. THE INTERSTELLAR EXTINCTION

In their discussion of the LMC distance, Benedict et al. (2002) pointed out that the average extinction-corrected magnitude of RR Lyrae variables in the LMC remains a significant uncertainty. Establishing the effect of interstellar extinction on the observed magnitudes of LMC stars is a difficult problem because the amount of extinction is not constant. Schwering & Israel (1991) found that the foreground reddening ranges from E(B-V)=0.07 to 0.17 mag over the LMC surface. Among the 16 fields in our study, their E(B-V) values range from approximately 0.07 to 0.14 mag. Thus it is not appropriate to make one reddening correction for all of the stars in our sample. It is more accurate to consider each star separately. Therefore, our approach is to calculate the effective temperatures from equation (5) and then use a color-temperature calibration to derive the unreddened colors. Equations relating $\log T_{eff}$ to $(V-R)_0$ have been derived by BG99 and by Kovács & Walker (1999, hereafter KW99). BG99's equations, which are based on model atmospheres of Castelli (1999), apply only for $\log g = 2.5$ and four different values of [Fe/H]. However, the temperature-color relation of KW99 is more general. They derived a linear expression (equation 10 in their paper) relating the temperature to color, $\log g$ and [M/H] based on models of Castelli, Gratton & Kurucz (1997):

$$\log T_{eff} = 3.8997 - 0.4892(V - R)_0 + 0.0113\log g + 0.0013[M/H]$$
(6)

and they also derived an expression (equation 12 in their paper) for estimating the gravity from mass, temperature and the fundamental mode pulsation period:

$$\log g = 2.9383 + 0.2297 \log M/M_{\odot} - 0.1098 \log T_{eff} - 1.2185 \log P_0. \tag{7}$$

We have used equations (4), (5), (6) and (7) to derive the unreddened color for each star. In each case, we assumed [M/H]=-1.5 and the fundamental mode pulsation period was computed from the overtone period (P_1) using a period ratio, $P_1/P_0 = 0.7445$. A plot of $\log T_{eff}$ versus (< V > - < R >) for the bona fide RR1 variables in each of the 16 fields is shown in Figure 14. The unreddened line in each panel is derived from equation (6) assuming $\log g = 2.9^{24}$ and [M/H]=-1.5. The diagram indicates that the color excess varies from field to field and also within the individual fields. Thus differential reddening may be responsible for at least some of the scatter in Figures 11 and 12. For each of the stars, we calculated the color excess and the corrected mean V magnitude:

$$E(V - R) = \langle V \rangle_F - \langle R \rangle_F - (V - R)_0 \tag{8}$$

 $^{^{24}}$ In order to plot the unreddened line in Figure 14, we calculated a mean value of $\log g$ for the 330 stars in our sample based on the mean $\log T_{eff}$ (3.863), the mean $\log M$ (-0.2085) and $\log P_0 = -0.3617$, which corresponds to the mean $\log P_1$ (-0.4898).

$$V_0(F) = \langle V \rangle_F -5.35E(V - R) \tag{9}$$

In Table 10, we summarize the mean $\langle V \rangle_F$, the mean extinction E(V-R) and the mean corrected magnitude $V_0(F)$ for the bona fide RR1 stars in each field. N is the number of RR1 stars in the field and in each case, the errors represent the standard error of the mean (i.e. the standard deviation divided by \sqrt{N}). In addition to these errors, there are systematic errors in E(V-R) and V_0 because of the uncertainties in the derivation of $\log T_{eff}$ and $(V-R)_0$. These will be discussed in section 5.2.

The temperature-color relations that BG99 derived apply only for $\log g = 2.5$ which is lower than the 2.9 that we have assumed. According to equation (6), the lower $\log g$ (2.5) would decrease $(V - R)_0$ by ~ 0.01 and thus increase the derived extinction. If we compare the $(V - R)_0$ colors derived from the BG99 relations with those predicted by our equation (6) for the same $\log g$ (i.e. 2.5), we find that the BG99 colors would be about 0.01 less for $T_{eff} \sim 7300$, a typical temperature for RR1 variables. Thus the extinction we derive for the same $\log g$ is lower than that predicted by BG99's equations.

On the other hand, the mean extinction we derive for our bona fide RR1 stars is larger than the value that C03 adopted for the same region. C03 observed RR Lyrae variables in two fields that overlap with our fields 6 and 13 for which we derived mean E(V-R) = 0.09 and 0.08 mag, respectively. This is equivalent to $E(B-V) \sim 0.15$ mag. They used two methods to determine the color excess for the stars in their sample. First, they used Sturch's (1966) method. For this, they compared the observed (B-V) colors of 62 RR0 (RRab) variables at minimum light with unreddened colors that were calculated from Walker's (1990) equation that relates color to period and metal abundance. The E(B-V) values that they derived for their fields A and B were 0.133 and 0.115 mag, respectively. In their second method, they derived the mean (B-V) colors for five RR Lyrae at the blue and five at the red edge of the instability strip and compared these with the colors Corwin and Carney (2001) observed for the instability strip boundaries in the globular cluster M3. To account for any color differences due to different metallicity, they applied a metallicitycolor shift relation derived by Walker (1998). Using this method, they derived E(B-V) = 0.116mag for their field A and 0.086 mag for field B, values that are lower than the ones they derived from the Sturch method. They adopted the latter values because independent studies of globular clusters have indicated that Sturch's method gives E(B-V) values that are about 0.02 mag larger than those determined by other techniques. The mean extinction we derived for fields 6 and 13 is comparable to what C03 found from the Sturch method, but considerably larger than the values they finally selected for their distance determination.

Nevertheless, our extinction values are comparable to what Udalski et al. (1999) adopted for the OGLE investigations of LMC RR Lyrae variables. Two of their fields (SC19 and SC20) overlap MACHO field 15. Initially, Udalski (1998) listed E(V-I)=0.26 mag for these two fields because this was the value used for the study of red clump stars (Udalski et al. 1998). It was based on a photometric (UBV) and spectroscopic study by Oestreicher & Schmidt-Kaler (1996). However, the region in question was not actually observed by these latter authors. It lies about two degrees

south of a region where they found high extinction. When Udalski et al. (1999) re-estimated the reddening for these fields from observations of red clump stars, they found that the extinction had been overestimated in the earlier study. Their revision indicates $E(V-I) \sim 0.23$ mag, which corresponds to $E(V-R) \sim 0.11$ mag, the mean extinction that we list for field 15 in Table 10.

Another bench mark for our extinction values is the recent study of LMC bump Cepheids by Keller & Wood (2002), based on MACHO data. Using pulsation theory, they derived the extinction for 20 stars, two of which were in field #19. The mean E(V-R) that they derived for these two stars, 0.03 mag, is the same mean that we have derived for this field. We can not consider this to be a conclusive result however, because their sample is so small.

5. THE M5-LIKE VARIABLES

5.1. The Selection of the M5-like Variables

Only the M5-like stars will be considered for our derivation of the LMC distance and we select these stars according to their location in the $\phi_{31} - \log P$ plots. Points that lie less than 2σ ($\Delta\phi_{31} = 0.214$) from the M5 line in Figure 8 are considered to be M5-like. (σ is the standard deviation of the fit of the K00 ϕ_{31} values to the line.) In Figure 15, we show $\phi_{31} - \log P$ plots for the individual fields with the lines for M5 and M68 superimposed. The stars that are plotted as crosses are the ones we classify as 'M5-like'. In column (2) of the electronic version of Table 1, these stars are denoted 'M'. The mean values of $\langle V \rangle_F$, extinction E(V - R) and $V_0(F)$ for the M5-like stars in each field are listed in the last three columns of Table 10. In each case, the quoted error is the standard error of the mean. These errors have been derived in the same manner as those listed in columns 3 to 5 of the table.

5.2. The Mean Apparent Magnitude of the M5-like Variables

In order to determine an LMC distance, we must derive the mean apparent magnitudes of the M5-like stars in our sample, correct these magnitudes for the effects of interstellar extinction and assess the errors. The mean $< V >_F$ and $< R >_F$ magnitudes listed in Table 10 are the mean A_0 values calculated from equation (1). The first step is to determine how well the A_0 values represent the data. To do this, we selected a subset of the M5-like stars, the ten in field 80, and applied Efron's bootstrap method (Diaconis & Efron 1983). The results indicated that the mean error in $A_0(V)$ was 0.0026 mag with a standard deviation of 0.0010. The equivalent numbers for $A_0(R)$ were 0.0034 and 0.0014 respectively. Thus, the errors in A_0 are very small. The next step is to compare A_0 with the 'intensity' mean magnitude ($< V >_{int}$) because in most studies of pulsating variable stars, the intensity means are used. To make this comparison, we calculated $< V >_{int}$ and $< R >_{int}$ for the same 10 stars and the results are presented in Table 11. It turns out that the

 A_0 values are generally about 0.01 mag fainter than the intensity means. We will take this into account when we adopt our final value for the mean corrected apparent magnitude.

In order to derive the interstellar extinction for each star, we need to determine the color. The mean colors listed in Tables 10 and 11 were computed from $(\langle V \rangle_F - \langle R \rangle_F)$. However, Fernie (1990) found that a straight average of the color over the pulsation cycle (e. g. $\langle V - R \rangle_{mag}$), is a better indicator of the temperature. We computed $\langle V - R \rangle_{mag}$ for the M5-like variables in field 80 and these are also listed in Table 11. The colors derived by the two methods differ by less than 0.01 mag. Thus we conclude that using $(\langle V \rangle_F - \langle R \rangle_F)$ to derive the extinction does not introduce any systematic errors. The main sources of error in E(V-R) are errors in the derived temperatures and in the color-temperature relation. Any errors in the observed colors are assumed to be minor and random, so that over the sample of 80 M5-like stars, they cancel out. On the other hand, the other two effects are not random because the stars in our sample have similar properties. Based on the errors in the fits of SC93's equations relating $\log L$ and $\log M$ of the pulsation models to the period and ϕ_{31} , ($\sigma_{\log L} = 0.035$ and $\sigma_{\log M} = 0.025$), we estimate that the error in $\log T_{eff}$ calculated from equation (5) is 0.01. This translates to an error of 0.02 mag in $(V-R)_0$. Since the dependence of log T_{eff} on ϕ_{31} is very weak, the errors in ϕ_{31} do not make a significant contribution to the errors in our derived temperatures. The discussion of the different $\log T_{eff}$ -color relations in section 4 indicates there is an additional uncertainty of ~ 0.01 mag in our $(V-R)_0$ colors. Adding in quadrature, we estimate that the systematic error in the color excess E(V-R) is 0.022 mag. Since $A_V = 5.35E(V - R)$, this propagates to an error of 0.12 mag in V_0 .

The distribution of $V_0(F)$ for the RR1 variables is shown in Figure 16. All of the 330 bona fide RR1 variables have been plotted, with the M5-like stars represented as solid areas. This diagram and the data in Table 10 both illustrate that the mean V_0 of the M5-like stars does not differ significantly from that of all of the RR1 variables. In Figure 16, each field is plotted separately in case there are systematic field-to-field variations. Within some of the individual fields, the range in V_0 for the M5-like stars is 0.5 mag or more. Based on the K00 study of M5, one would expect a scatter of at least 0.1 mag in V_0 among the M5-like variables. Some of the additional scatter must be due to variations in distance from the observer, but some is probably caused by crowding. Artificial star tests in the MACHO fields support this conclusion. The results from these tests will be discussed further in section 5.4 where we estimate the LMC distance using M5-like stars, and include a correction for crowding bias. Figure 17, a plot of $\langle V_0 \rangle_F$ versus the density for each field, also illustrates that crowding affects our derived V_0 values. One would not expect a perfect correlation in Figure 17 because it is possible for stars in low density fields to have unresolved companions. Nevertheless, the faintest mean V_0 (~ 19.1) occurs in low density fields, and the mean V_0 is ~ 0.3 mag brighter in the highest density fields where the crowding is expected to be the most severe. Although we have tried to overcome the crowding problem by restricting our sample to stars with an amplitude ratio A_R/A_V between 0.75 and 0.85, it appears that it has not been completely eliminated.

Another method for checking our adopted mean magnitudes is to compare with other investi-

gations. Seven of the bona fide RR1 stars from Table 1 were included in C03's study. Their mean magnitudes will be published in a forthcoming paper by Di Fabrizio et al. (2003). In Table 12, we list the mean < V > magnitudes derived for these stars from the two studies; for both groups, the means that we list are arithmetic means. The average of the C03 mean magnitudes is 0.07 mag fainter than ours. It is more difficult to compare our results with those of Udalski et al. (1999) because most of the OGLE observations were in the I band and the mean magnitudes that they published were corrected for extinction. In addition, the mean that they quoted included RR Lyrae variables in four different LMC fields. In Udalski's 1998 study, a mean $V_0 = 18.86$ mag was adopted for 110 RR0 variables in these fields, two of which overlap with our field 15. This mean was derived from ~ 65 I and 6 V magnitudes for each star. Later, when more observations were available for these stars (~ 140 in the I-band and 20 in the V-band) and the extinction was revised, Udalski et al. (1999) changed the mean V_0 to 18.94 ± 0.04 . The mean $< V_0 >$ that we list in Table 10 for the 13 stars in field 15 is 19.00 ± 0.13 .

5.3. The Absolute Magnitudes of the M5-like Variables

In our derivation of the absolute magnitude, we consider four independent methods: Baade-Wesselink (B-W) analysis, main sequence fitting, trigonometric parallax of the star RR Lyrae and Fourier analysis.

As we noted at the end of section 3.2, Storm et al. (1994) performed a B-W analysis of two RR Lyrae variables (V8 and V28) in M5. They derived $M_V = 0.65$ and 0.67 mag, using a value of 1.30 for p, the conversion factor between observed and true pulsation velocity. Later, Clementini et al. (1995) revised these values to $M_V = 0.52 \pm 0.26$ and 0.54 ± 0.26 mag, by assuming [Fe/H]= -1.17 and p = 1.38. However, if the assumed metal abundance is less, e.g. the ZW value of -1.40 instead of -1.17, these stars would be 0.02 mag fainter. The adopted p-factor (1.38) is the value that gives the brightest possible value of the luminosity and Fernley (1994) considered it to be a more appropriate value than 1.30. More recently, Cacciari et al. (2000) re-examined the calibration of B-W results and suggested that p might be a few percent smaller than 1.38. Based on all of this, we adopt $M_V(BW) = 0.55 \pm 0.26$ mag for the M5 RR Lyrae variables.

Carretta et al (2000) derived $M_V = 0.54 \pm 0.09$ mag for the HB of M5 by fitting the main sequence to subdwarfs with parallaxes determined from Hipparcos. However, Gratton et al. (2002, 2003) have subsequently concluded that this is too bright. Using the ESO VLT telescopes, they made new spectroscopic observations of subdwarfs in the Galactic field and in the three globular clusters NGC 6397, NGC 6752 and 47 Tuc and have revised the metal abundances. They also derived new reddening values. The new data indicate that the absolute V magnitude for the horizontal branch of M5 may be as bright as 0.58 or as faint as 0.65, depending on the assumed metal abundance. We adopt $M_V(HB) = 0.61 \pm 0.12$ mag.

Benedict et al. (2002) used HST astrometry to derive a trigonometric parallax for RR Lyrae

and then calculated its absolute magnitude: $M_V = 0.61^{-0.11}_{+0.10}$. Because of the location of RR Lyrae in a period-amplitude plot, we assume that its absolute magnitude is comparable to that of an M5 RR Lyrae variable. It is well known that the light curve of the star, RR Lyrae ($P = 0^{d}.567$), is modulated with a longer secondary period (~ 40 days), i.e. it exhibits the Blazkho effect (Smith 1995). However, according to Szeidl (1988), the maximum light amplitude of a Blazhko variable always fits the period-amplitude relation for singly periodic variables. According to some recently published observations of RR Lyrae (Smith et al. 2003), its maximum V amplitude is ~ 0.9 mag, which places it on the period-amplitude relation that K00 plotted for the RR0 variables in M5. If there is a period-luminosity-amplitude relation for RR0 variables as demonstrated by Sandage (1981), then we may assume that the absolute magnitude of RR Lyrae is comparable to that of an M5-like variable. We adopt $M_V(\text{trig }\pi) = 0.61^{+0.10}_{-0.11}$ mag.

Equations (2) and (3), which were derived by SC93 and K98 respectively, show relationships between Fourier coefficients and the luminosity of RR1 variables. K98 based the zero-point for his equation on absolute magnitudes derived from B-W analyses of field and cluster RR Lyrae variables. We have already taken into account the B-W analyses of two RR Lyrae variables in M5, but we can not assume that the other stars for which B-W analyses have been carried out, and on which K98 based his zero point, have properties similar to the RR Lyrae in M5. Therefore, we will not derive an absolute magnitude from equation (3), we will consider only equation (2). The mean $\log L/L_{\odot}$ for the 80 M5-like stars in our sample is 1.688. Assuming that the Sun's $M_{bol} = 4.74$ (BG99), we derive a mean $< M_{bol} >= 0.52$ for these M5-like stars. From the $BC - (V - R)_0$ plot of BG99, we read BC = 0.02 at $[Fe/H] \sim -1.5$ and $(V - R)_0 = 0.14$ (a typical color for an RR1 variable). Since the standard deviation of the fit of equation (2) to SC93's models was $\sigma_{\log L} = 0.035$, the mean M_V derived from ϕ_{31} is 0.50 ± 0.09 mag.

Using a weighted average of these four values, our final adopted mean M_V for M5-like RR Lyrae variables is 0.56 ± 0.06 mag.

5.4. The LMC Distance

The average $V_0(F)$ for the 80 M5-like stars is 18.91 ± 0.02 where the quoted error is the standard error of the mean. If the $< V_0 >$ values for the individual fields are corrected for D/D_0 , this is revised to 18.89 ± 0.02 . We emphasize that making this correction assumes that the RR Lyraes lie in the main disk of the LMC. Fortunately, since our stars lie near the center of the LMC, the difference between the two values is small. Because of the systematic difference between $A_0(V)$ and $< V>_{int}$, we subtract 0.01 from $< V_0(F) >$ and adopt a mean V_0 of 18.88 ± 0.02 for the 80 M5-like stars in our 16 fields. In addition, there is a systematic error of 0.12 mag due to the uncertainty in E(V-R). We must also account for crowding bias which is known to exist in the MACHO data because of the artificial star tests.

As the final step in calculating the LMC distance, we estimate a correction for the apparent

brightness of the RR1 stars using artificial star tests that were part of the MACHO microlensing detection efficiency calculation (Alcock et al. 2001). This calculation is fraught with difficulty because many of the steps in the process of selecting bona fide RR1 variables, for example the removal of severely blended stars, cannot be modeled accurately. Therefore, our approach is to interpret the artificial star tests in two different ways, and thus derive two magnitude corrections for the RR1 stars. The difference between the two estimates obtained is taken to indicate the level of systematic error associated with the final adopted magnitude correction, and hence also with our LMC distance result.

The MACHO artificial star tests were made in 10 regions of the LMC that span the range of different crowding conditions found in the MACHO database. The parameter that we adopt as a measure of the crowding is the number of objects detected per square arcminute, or what we call the 'Density' in Table 8 (see also Tables 1 & 2 of Alcock et al. 2001). In the most crowded MACHO fields, this 'Density' may have been underestimated because it is more difficult to detect the faint objects. The correction that we seek, ΔV , is the difference between the input and recovered magnitudes of the artificial stars. For our first method, we calculated the average ΔV for stars in 4 (1-mag wide) bins centered at V = 17.5, 18.5, 19.5, and 20.5 mag. A high order polynomial function was fit to these binned data points in order to predict ΔV in terms of recovered magnitude and field density for any value of these two parameters. Since the frequency-weighted mean density for the M5-like RR1 stars in our sample is 200 objects/arcmin², we evaluated the function for a density of 200 objects/arcmin² and derived ΔV (recovered – input) = -0.21 mag at V = 19.3. However, because we used an (unclipped) straight average for ΔV in each bin, heavily blended artificial stars may tend to inflate the correction. In fact this correction is probably an upper limit for the RR1 stars in our sample because we have already removed the most severely blended stars, but these are given full weight when interpreting the artificial stars. For our second estimate, we constructed one bin of artificial stars with V=19.1 to 19.5 mag and calculated the median ΔV value at each of the 10 different field densities. A second-order polynomial that was forced to pass through zero in an empty field was fit to these data.²⁵ In this case, $\Delta V = -0.11 \pm 0.10$ mag at a density of 200 object/arcmin². Since the median value is not significantly affected by outlying points like those due to severe blends, we believe that this approach is more appropriate for our data. When this correction is applied, our V_0 is revised to 18.99 mag. In section 5.2 and Table 12, we showed that our mean V magnitudes for seven RR1 stars in fields #6 and #13 appear to be ~ 0.07 brighter than those of C03. When the crowding correction for these two fields is applied to the MACHO magnitudes for these stars, the mean V magnitude for the MACHO data is 0.03 mag fainter than the C03 values, well within the estimated errors.

There are two sources of systematic error in our estimate of V_0 . The first is the error in our derived $(V - R)_0$ color (0.022 mag) which propagates to an error of 0.12 mag in V_0 . The second is the error in our crowding correction (0.10 mag). Combining these in quadrature, we estimate that

²⁵For V = 19.1 to 19.5 mag, $\Delta V = -6.06 \times 10^{-5} \cdot O - 2.34 \times 10^{-6} \cdot O^2$, where O is objects/arcmin².

the systematic error in V_0 is 0.16 mag. Another factor that should be considered is the effect of crowding on the derived Fourier coefficients. To address this problem, SC93 performed simulations in which they added constant light to the observed magnitudes at all phases on the light curves. They found that, although A_0 brightened, ϕ_{31} remained largely unaltered. We therefore conclude that crowding has not seriously affected our selection of the 'M5-like' stars.

The final mean LMC distance modulus that we obtain for the 80 M5-like RR1 variables, based on $M_V = 0.56$ and $V_0 = 18.99$, is $\mu_{LMC} = 18.43 \pm 0.06$ (statistical) ± 0.16 (systematic). Our analysis has illustrated that the two major impediments to the derivation of a precise LMC distance from RR Lyrae variables are the uncertainty in the extinction and the uncertainty in establishing the effects of light contamination due to crowding. Near-infrared photometry (see, for example, the recent study of the Reticulum cluster by Dall'Ora et al. 2003) is an effective way to deal with the first problem. To address the second problem, investigations like the SuperMACHO project which is based on observations obtained with the 4-meter telescope at Cerro Tololo will provide images with better resolution. Preliminary results indicate that the median seeing of the CTIO images is a factor of three smaller than the FWHM of the images that were obtained with the Mt. Stromlo 50-inch telescope for the MACHO project.

6. SUMMARY

We have determined Fourier coefficients for 785 stars deemed to be first-overtone RR Lyrae (RR1) variables according to their periods, magnitudes and colors. We established that 330 of these stars are bona fide RR1 stars. By using a $\phi_{31} - \log P$ plot, we compared the LMC stars with the RR1 variables in some well-studied GGCs and found that they have properties similar to the ones in M2, M3, M5 and the OoI variables in ω Centauri. However, they are different from the OoII variables in ω Cen. In addition, there are a significant number that do not have counterparts in the well-studied GGCs.

There are several problems that must be addressed in deriving the LMC distance from RR Lyrae variables. Perhaps the most important is the correction for differential extinction. We have shown that there is a large range in the color excess from field to field (0.03 < E(V - R) < 0.13), in good agreement with the results of other studies. We also found a significant variation among the stars within individual fields. These variations indicate that it is advantageous to correct for the extinction on a star-by-star basis. We did this by computing the temperature of each star from ϕ_{31} and $\log P$ and then using the temperature to derive the unreddened color.

Another consideration is that the star fields in the LMC, particularly those in the region of the bar, are extremely crowded. By comparing the V and R pulsation amplitudes, we removed the most severely blended stars from our sample. Further, a statistical correction based on artificial star tests was made to rectify the photometric errors caused by more moderate blending.

Finally, it is important to select a homogeneous group of stars for which the absolute magnitude

is well-determined. To do this, we identified the 'M5-like' RR1 stars in our sample and applied absolute magnitudes determined from four independent methods to derive a distance modulus of 18.43 ± 0.06 (statistical) ± 0.16 (systematic) mag. This method has the advantage that the result does not depend on the still somewhat uncertain M_V – [Fe/H] relation for RR Lyrae variables.

We are very grateful for the skilled support given our project by the technical staff at the Mt. Stromlo Observatory. In addition, it is a pleasure to thank Ed Guinan and Gisella Clementini for valuable discussions with CMC during the preparation of this paper. Gisella responded cheerfully and promptly to the many questions we asked and provided us with some of her unpublished results. This work was performed under the auspices of the U.S. Department of Energy, National Nuclear Security Administration by the University of California, Lawrence Livermore National Laboratory under contract No. W7405-ENG-48, the National Science Foundation through the Centre for Particle Astrophysics of the University of California under cooperative agreement AST-8809616, and the Mount Stromlo and Siding Springs Observatory by the Bilateral Science and Technology Program of the Australian Department of Industry, Technology and Regional Development. CMC and DLW were supported by the Natural Sciences and Engineering Research Council of Canada (NSERC). AM and JFR held NSERC Undergraduate Student Research Awards during this work. KG and TV were supported in part by the Department of Energy under grant DEF03-90-ER 40546. DM is supported by FONDAP Center for Astrophysics 15010003.

REFERENCES

Alcock, C. et al. 1996, AJ, 111, 1146 (A96)

Alcock, C. el al. 1999 PASP, 111, 1539 (A99)

Alcock, C. et al. 2000, ApJ, 542, 257 (A00)

Alcock, C. et al. 2001, ApJS, 136, 439

Alcock, C. et al. 2003, VizieR On-line Data Catalog: II/247

Allsman, R. A. & Axelrod, T. S. 2001, astro-ph/0108444

Alves, D. R., Rejkuba, M., Minniti, D., & Cook, K. H. 2002, ApJ, 573, L51

Bragaglia, A., Gratton, R. G., Carretta, E., Clementini, G., Di Fabrizio, L., & Marconi, M. 2001, AJ, 122, 207

Benedict, G. F., et al. 2002, AJ, 123, 473

Bessell, M. S. & Germany, L.M. 1999, PASP, 111, 1421 (BG99)

Bono, G., Caputo, F., Castellani, V., & Marconi, M. 1997, A&AS, 121, 327

Cacciari, C., Clementini, G., Castelli, F., & Melandri, F. 2000, in IAU Colloq. 176, The Impact of Large-Scale Surveys on Pulsating Star Research, ed. L. Szabados & D. W. Kurtz (ASP Conf. Ser. 203, San Francisco: ASP), 176

Carretta, E., Gratton, R. G., Clementini, G., & Fusi Pecci, F. 2000, ApJ, 533, 215

Castelli, F. 1999, A&A, 346, 564

Castelli, F., Gratton, R. G., & Kurucz, R. L. 1997, A&A, 318, 841

Clement, C. M., Jankulak, M., & Simon, N. R. 1992, ApJ, 395, 192

Clement, C. & Rowe, J. 2000, AJ, 120, 2579

Clement, C. M. & Shelton, I. 1997, AJ, 113, 1711

Clement, C. M., et al. 2001, AJ, 122, 2587

Clementini, G., Carretta, E., Gratton, R., Merighi, R., Mould, J. R., & McCarthy, J. K. 1995, AJ, 110, 2319

Clementini, G., Gratton, R., Bragaglia, A., Carretta, E., Di Fabrizo, L., & Maio, M. 2003, AJ, 125, 1309 (C03)

Corwin, T. M. & Carney, B. W. 2001, AJ, 122, 3183

Dall'Ora, M. et al. 2003, astro-ph/0305276

Diaconis, P. & Efron, B. 1983, Sci. Am., 248, No. 5, 116

Di Fabrizio, L. et al. 2003, (in preparation)

Fernie, J. D. 1990, ApJ, 354, 295

Fernley, J. 1994, A&A, 284, L16

Freedman, W. L. et al. 2001, ApJ, 553, 47

Gratton, R. G., Bragaglia, A., Carretta, E., Clementini, G., & Grundahl, F. 2002, in New Horizons on Globular Cluster Astronomy, ed. G. Piotto, G. Meylan, S. G. Djorgovski, & M. Riello (ASP Conf. Ser. 296, in press, San Francisco: ASP)

Gratton, R. G., Bragaglia, A., Carretta, E., Clementini, G., Desidera, C., Grundahl, F., & Lucatello, S. 2003, astro-ph/0307016, (A&A, in press)

Harris, W. E. 1996, AJ, 112, 1487

Kałużny, J., Hilditch, R. W., Clement, C., & Ruciński, S. M. 1998, MNRAS, 296, 347

Kałużny, J., Kubiak, M., Szymański, A., Udalski, A., Krzemiński, W., Mateo, M. & Stanek, K. 1997, A&AS, 125, 343

Kałużny, J., Olech, A., Thompson, I., Pych, W., Krzemiński, W., & Schwarzenberg-Czerny, A. 2000, A&AS, 143, 215 (K00)

Keller, S. C. & Wood, P. R. 2002, ApJ, 578, 144

Kovács, G. 2000, in The Impact of Large-Scale Surveys on Pulsating Star Research, IAU Colloq. 176, ed. L. Szabados & D. W. Kurtz (ASP Conf. Ser. 203; San Francisco: ASP), 313

Kovács, G. 1998, Mem. Soc. Astron. Italiana, 69, 49 (K98)

Kovács, G. & Walker, A. R. 1999, ApJ, 512, 271 (KW99)

Lee, J.-W. & Carney, B. W. 1999, AJ, 117, 2868 (LC99)

Mitchell, R. C., Baron, E., Branch, D., Hauschildt, P. H., Nugent, P. E., Lundqvist, P., Blinnikov, S., & Pun, C. S. J. 2002, ApJ, 574, 293

Oestreicher, M. O. & Schmidt-Kaler, Th. 1996, A&AS, 117, 303

Olech, A., Kałużny, J., Thompson, I. B., Pych, W., Krzemiński, W., & Schwarzenberg-Czerny, A. 1999, AJ, 118, 442

Oosterhoff, P. Th. 1939, Observatory, 62, 104

Oosterhoff, P. Th. 1944, Bull. Astron. Inst. Netherlands, 10, 55

Petersen, J. O. 1984, A&A, 139, 496

Pritzl, B. J., Smith, H. A., Catelan, M., & Sweigart, A. V. 2001, AJ, 122, 2600

Sandage, A. 1981, ApJ, 244, L23

Schlegel, D. J., Finkbeiner, D. P., & Davis, M. 1998, ApJ, 500, 525

Schwering, P. B. W. & Israel, F. P. 1991, A&A, 246, 231

Simon, N. R. & Clement, C. M. 1993, ApJ, 410, 526 (SC93)

Simon, N. R. & Moffett, T. J. 1985, PASP, 97, 1078

Simon, N. R. & Teays, T. J. 1982, ApJ, 261, 586

Smith, H. A. 1995, RR Lyrae Stars (Cambridge University Press, Cambridge)

Smith, H. A., Church, J. A., Fournier, J., Lisle, J., Gay, P., Kolenberg, K., Carney, B. W., Dick, I., Petersen, R. C., & Hakes, B. 2003, PASP, 115, 43

Spergel, D. N. et al. 2003, astro-ph/0302209 (version accepted to ApJ)

Stellingwerf, R. F. 1978, ApJ, 224, 953

Storm, J., Carney, B. W., & Latham D. W. 1994, A&A, 290, 443

Sturch, C. 1966, ApJ, 143, 774

Szeidl, B. 1988, in Multimode Stellar Pulsations, ed. G. Kovács, L. Szabados, & B. Szeidl (Budapest: Konkoly Observatory), 45

Udalski, A. 1998, Acta Astron. 48, 113

Udalski, A., Szymański, M., Kubiak, M., Pietrzyński, G., Woźniak, P., & Żebrunń, K. 1998, Acta Astron. 48, 1

Udalski, A., Szymański, M., Kubiak, M., Pietrzyński, G., Soszyński, I., Woźniak, P., & Żebrunń, K. 1999, Acta Astron. 49, 201

van der Marel, R. P. 2001, AJ, 122, 1827

van der Marel, R. P. & Cioni, M. L. 2001, AJ, 122, 1807 (vMC01)

Walker, A. R. 1990, AJ, 100, 1532

Walker, A. R. 1994, AJ, 108, 555

Walker, A. R. 1998, AJ, 116, 220

Yoon, S.-J. & Lee, Y.-W. 2002, Science, 297, 578

Zinn, R. & West, M. J. 1984, ApJS, 55, 45 (ZW)

This preprint was prepared with the AAS IATEX macros v5.0.

TABLE CAPTIONS

- Table 1. Fourier Parameters of LMC RR1 Variables
- Table 2. Fourier Parameters of LMC RR01 Variables
- Table 3. Fourier Parameters of LMC RR12 Variables
- Table 4. Fourier Parameters of LMC RR1- ν 1 Variables
- Table 5. Fourier Parameters of Other Multifrequency LMC RR1 Variables
- Table 6. LMC RR1 Variables Included in Two Fields
- Table 7. Blended or Foreground RR1 Variables
- TABLE 8. MEAN MAGNITUDES AND COLORS OF LMC RR1 VARIABLES BY FIELD
- Table 9. Fourier Parameters for the RR1 Variables in M2
- Table 10. Corrected Magnitudes and Reddenings by Field
- Table 11. Mean Magnitudes and Colors for the M5-like Stars in Field 80
- Table 12. Mean Magnitudes for Stars Observed by C03

Table 1. Fourier Parameters of LMC RR1 Variables

Color & Star# N_{obs}	Period Amplitude	A_0	A_1	R_{21}	R_{31}	R_{41}	ϕ_{21}	ϕ_{31}	ϕ_{41}
(1)	(2)	σ_{fit} (3)	(4)	(5)	(6)	σ (7)	(8)	(9)	(10)
V80.6589.1879	0.249987	19.24	0.149	0.1129	0.0324	0.0318	4.81	3.36	1.87
751	0.304	0.066		0.0236	0.0238	0.0244	0.22	0.74	0.75
R80.6589.1879	0.249987	18.94	0.104	0.1198	0.0359	0.0546	4.56	2.39	2.16
736	0.213	0.071		0.0368	0.0371	0.0378	0.32	1.05	0.69
V2.5389.1478	0.250557	19.52	0.178	0.0679	0.0611	0.0117	4.99	3.04	4.03
469	0.358	0.082		0.0303	0.0310	0.0299	0.46	0.51	2.69
R2.5389.1478	0.250557	19.30	0.136	0.1228	0.0481	0.0561	4.57	3.54	4.59
455	0.286	0.074		0.0353	0.0366	0.0354	0.32	0.75	0.67
V6.5849.1114	0.255347	19.55	0.189	0.1462	0.0593	0.0161	4.39	3.43	3.23
363	0.391	0.060		0.0247	0.0235	0.0239	0.17	0.41	1.48
R6.5849.1114	0.255347	19.36	0.147	0.1217	0.1044	0.0546	4.62	3.99	1.38
372	0.284	0.059		0.0302	0.0298	0.0293	0.25	0.30	0.57

Note. — Table 1 is available in its entirety in the electronic edition of the Astronomical Journal. A portion is shown here for guidance regarding its form and content.

Table 2. Fourier Parameters of LMC RR01 Variables

Color & Star# N_{obs}	Period Amplitude	A_0	A_1	R_{21}	R_{31}	R_{41} σ	ϕ_{21}	ϕ_{31}	ϕ_{41}
(1)	(2)	σ_{fit} (3)	(4)	(5)	(6)	(7)	(8)	(9)	(10)
V80.7193.1485	0.328817	19.50	0.215	0.1431	0.0766	0.0157	5.14	4.98	1.23
514	0.433	0.084		0.0244	0.0248	0.0249	0.18	0.34	1.62
R80.7193.1485	0.328817	19.24	0.168	0.1701	0.1139	0.0528	4.99	5.33	5.55
394	0.379	0.099		0.0409	0.0430	0.0428	0.28	0.40	0.85
V81.8639.1450	0.335260	19.14	0.124	0.1152	0.1500	0.0356	4.35	2.77	1.21
435	0.256	0.069		0.0380	0.0389	0.0386	0.34	0.28	1.07
R81.8639.1450	0.335260	18.92	0.101	0.1169	0.0766	0.0296	4.21	3.10	4.66
466	0.203	0.068		0.0449	0.0455	0.0447	0.39	0.59	1.56

Note. — Table 2 is available in its entirety in the electronic edition of the Astronomical Journal. A portion is shown here for guidance regarding its form and content.

Table 3. Fourier Parameters of LMC RR12 Variables

Color & Star# N_{obs}	Period Amplitude	A_0	A_1	R_{21}	R_{31}	R_{41}	ϕ_{21}	ϕ_{31}	ϕ_{41}
(1)	(2)	σ_{fit} (3)	(4)	(5)	(6)	(7)	(8)	(9)	(10)
V12.10443.367	0.336557	18.91	0.099	0.1408	0.1096	0.0261	1.30	6.16	3.10
674	0.215	0.056		0.0320	0.0319	0.0311	0.23	0.30	1.22
R12.10443.367	0.336557	18.60	0.076	0.1588	0.1035	0.0541	1.73	0.29	3.80
725	0.174	0.057		0.0400	0.0406	0.0399	0.26	0.39	0.75
V12.10202.285	0.398113	18.76	0.111	0.2345	0.2008	0.0918	2.11	0.09	4.14
565	0.262	0.056		0.0313	0.0314	0.0316	0.15	0.17	0.34
R12.10202.285	0.398113	18.43	0.092	0.2535	0.2196	0.0843	2.19	0.32	4.42
601	0.216	0.052		0.0341	0.0343	0.0344	0.15	0.17	0.41

Table 4. Fourier Parameters of LMC RR1- ν 1 Variables

Color & Star#	Period	A_0	A_1	R_{21}	R_{31}	R_{41}	ϕ_{21}	ϕ_{31}	ϕ_{41}
N_{obs} (1)	Amplitude (2)	σ_{fit} (3)	(4)	(5)	(6)	(7)	(8)	(9)	(10)
V14.9702.401	0.275403	19.39	0.224	0.1919	0.0823	0.0562	4.50	2.62	1.42
532	0.455	0.067		0.0187	0.0181	0.0182	0.10	0.24	0.34
R14.9702.401	0.275403	19.23	0.183	0.2491	0.0787	0.0460	4.51	2.52	1.18
539	0.389	0.063		0.0216	0.0207	0.0209	0.09	0.28	0.47
V6.5730.4057	0.276320	19.41	0.117	0.2582	0.0262	0.0478	4.18	2.61	2.10
519	0.262	0.075		0.0416	0.0415	0.0402	0.19	1.53	0.88
R6.5730.4057	0.276320	19.30	0.100	0.2406	0.0803	0.0455	4.25	2.14	1.76
483	0.218	0.068		0.0450	0.0451	0.0446	0.22	0.57	1.01

Note. — Table 4 is available in its entirety in the electronic edition of the Astronomical Journal. A portion is shown here for guidance regarding its form and content.

Table 5. Fourier Parameters of Other Multifrequency LMC RR1 Variables

Color & Star# N_{obs}	Period Amplitude	A_0	A_1	R_{21}	R_{31}	R_{41}	ϕ_{21}	ϕ_{31}	ϕ_{41}
$ \begin{array}{c} $	(2)	σ_{fit} (3)	(4)	(5)	(6)	σ (7)	(8)	(9)	(10)
V3.6243.404	0.270850	19.41	0.196	0.2331	0.0761	0.2712	4.64	3.29	2.23
128	0.467	0.101		0.0826	0.0812	0.0738	0.33	1.07	0.47
R3.6243.404	0.270850	19.19	0.168	0.1906	0.1450	0.1716	4.93	2.38	1.88
189	0.362	0.085		0.0548	0.0563	0.0562	0.29	0.42	0.37
V80.7441.933	0.273310	19.28	0.165	0.1864	0.0331	0.0491	4.61	3.37	2.49
369	0.349	0.098		0.0464	0.0446	0.0441	0.25	1.33	0.92
R80.7441.933	0.273310	19.04	0.141	0.1653	0.1261	0.0518	4.62	3.34	2.80
359	0.292	0.068		0.0376	0.0363	0.0359	0.23	0.31	0.72

Note. — Table 5 is available in its entirety in the electronic edition of the Astronomical Journal. A portion is shown here for guidance regarding its form and content.

Table 6. RR Lyrae Stars Included in Two Fields

Star	RA	DEC	Period (days)	$< V >_F$	$< R >_F$	$\phi_{31} \pm \sigma$ (V)	Table no.
10.4400.4594	05:07:39.804	-69:58:26.57	0.332233	19.26	19.04	3.63 ± 0.33	1
5.4400.1081	05:07:40.150	-69:58:27.11	0.332233	19.24	19.06	4.19 ± 0.30	1
19.4789.4120	05:09:39.150	-68:15:00.80	0.326913	19.32	19.13	3.60 ± 0.35	1
2.4789.946	05:09:39.189	-68:15:00.44	0.326910	19.23	19.05	3.20 ± 0.17	1
6.5721.289	05:15:37.913	-70:37:50.48	0.335580	19.14	18.93	2.90 ± 0.19	1
13.5721.2108	05:15:38.028	-70:37:50.15	0.335580	19.16	18.94	2.59 ± 0.20	1
13.5965.3725	05:17:08.129	-70:31:19.35	0.316960	19.31	19.07	2.70 ± 0.27	1
6.5965.835	05:17:08.279	-70:31:19.29	0.316963	19.32	19.11	3.12 ± 0.21	1
13.6084.2519	05:18:09.290	-70:38:12.73	0.306750	19.40	19.15	2.24 ± 0.24	1
6.6084.462	05:18:09.305	-70:38:12.43	0.306747	19.41	19.15	2.78 ± 0.23	1
13.6569.4284	05:21:14.235	-70:34:00.52	0.315017	19.45	19.23	3.29 ± 0.28	1
6.6569.955	05:21:14.199	-70:34:00.34	0.315017	19.44	19.23	2.83 ± 0.19	1
13.6689.3055	05:21:33.252	-70:39:52.25	0.305057	19.25	19.03	2.54 ± 0.22	1
6.6689.563	05:21:33.487	-70:39:51.81	0.305057	19.24	19.03	2.40 ± 0.15	1
80.6839.4533	05:22:22.451	-68:44:58.54	0.304307	19.77	19.52	2.58 ± 0.11	1
3.6839.2292	05:22:22.497	-68:44:57.87	0.304307	19.75	19.52	2.63 ± 0.20	1
80.7201.3035	05:24:42.268	-68:47:00.97	0.319110	19.12	18.84	2.18 ± 0.16	1
3.7201.504	05:24:42.314	-68:47:01.52	0.319110	19.24	18.95	2.24 ± 0.19	1
11.8744.752	05:33:59.600	-70:48:10.99	0.280960	19.19	19.05	2.60 ± 0.35	1
14.8744.3856	05:33:59.777	-70:48:13.29	0.280957	19.22	19.07	2.68 ± 0.27	1
11.8863.163	05:35:05.584	-70:54:04.95	0.331207	19.56	19.40	2.51 ± 0.13	1
14.8863.1362	05:35:05.812	-70:54:05.05	0.331207 0.331203	19.54	19.37	2.53 ± 0.13 2.53 ± 0.23	1

Table 6—Continued

Star	RA	DEC	Period	$< V >_F$	$< R >_F$	$\phi_{31} \pm \sigma$	Table no.
			(days)			(V)	

Note. — $\langle V \rangle_F$ and $\langle R \rangle_F$ denote $A_0(V)$ and $A_0(R)$ which were derived from the fits of equation (1) to the observations. Table 6 is available in its entirety in the electronic edition of the Astronomical Journal. A portion is shown here for guidance regarding its form and content. The 11 pairs of stars listed above are all considered to be bona fide RR1 variables.

Table 7. Blended or Foreground RR1 Variables

Star (1)	Period (2)	A(V) (3)	$\langle V \rangle_F$ (4)	$\langle R \rangle_F$ (5)	$\langle V \rangle_F - \langle R \rangle_F$ (6)
(1)	(2)	(0)	(4)	(0)	(0)
2.5873.332	0.2965	0.27	18.74	18.40	0.34
2.5148.713	0.3213	0.34	18.96	18.65	0.31
2.5752.387	0.4592	0.37	18.66	18.37	0.29
3.7450.214	0.3919	0.26	18.98	18.65	0.33
5.5252.708	0.3663	0.39	18.81	18.53	0.28
6.6576.558	0.2692	0.20	18.74	18.37	0.37
6.5851.3773	0.3210	0.35	18.77	18.45	0.32
6.6811.481	0.3560	0.35	18.86	18.56	0.30
11.9111.591	0.3146	0.24	19.04	18.69	0.35
13.6438.48	0.2937	0.27	18.96	18.60	0.36
19.4303.852	0.2617	0.24	18.76	18.46	0.30
80.6950.6196	0.3022	0.43	19.07	18.73	0.34
80.7315.1237	0.3191	0.30	18.92	18.62	0.30
80.7313.3932	0.3406	0.42	19.10	18.73	0.37
80.7192.4319	0.3496	0.32	19.02	18.61	0.41
80.7436.1309	0.3692	0.29	18.89	18.59	0.30
81.8639.662	0.2853	0.26	18.70	18.35	0.35

Table 8. Mean Magnitudes and Colors of LMC RR1 Variables by Field

Field	ρ	Φ	D/D_0	Density	$< V >_F$	$\langle R \rangle_F$	Color	N_{RR}
(1)	(2)	(3)	(4)	(5)	(6)	$ \operatorname{Mean}/\sigma - (7)$	(8)	(9)
2	1.77°	304°	0.9999	184.7	19.30/0.21	19.09/0.20	0.21/0.04	66
3	1.21°	331°	0.9933	173.4	19.50/0.25	19.22/0.24	0.27/0.04	37
5	1.56°	262°	1.0128	237.9	19.26/0.18	19.06/0.17	0.20/0.04	55
6	1.12°	223°	1.0137	226.4	19.36/0.18	19.14/0.18	0.22/0.05	84
10	2.17°	257°	1.0198	182.3	19.30/0.18	19.09/0.17	0.21/0.03	34
11	1.25°	147°	1.0065	221.9	19.41/0.23	19.22/0.21	0.20/0.06	43
12	1.79°	129°	1.0029	202.9	19.40/0.17	19.16/0.16	0.24/0.04	22
13	1.58°	209°	1.0198	179.6	19.33/0.14	19.11/0.13	0.22/0.04	78
14	1.76°	161°	1.0139	211.1	19.29/0.15	19.11/0.14	0.18/0.04	27
15	2.25°	143°	1.0104	182.9	19.53/0.14	19.28/0.14	0.25/0.04	24
18	2.82°	278°	1.0156	214.0	19.29/0.18	19.09/0.18	0.20/0.04	22
19	2.37°	297°	1.0036	169.6	19.24/0.15	19.06/0.15	0.18/0.04	26
47	3.58°	290°	1.0114	141.7	19.25/0.16	19.07/0.13	0.19/0.04	17
80	0.69°	308°	0.9993	237.9	19.37/0.19	19.10/0.18	0.27/0.04	54
81	0.70°	116°	0.9991	210.6	19.39/0.28	19.17/0.26	0.22/0.05	38
82	0.58°	39°	0.9931	170.4	19.38/0.18	19.12/0.17	0.26/0.04	37
\mathbf{ALL}					19.35/0.20	19.13/0.19	0.22/0.05	663

Table 9. Fourier Parameters of M2 RR1 Variables

Star	Period N	$A_0 \\ A_v$	A_1	R_{21}	R_{31}	R_{41} $\sigma =$	ϕ_{21}	ϕ_{31}	ϕ_{41}	
(1)	(2)	(3)	σ_{fit} (4)	(5)	(6)	(7)	(8)	(9)	(10)	
V19	0.319416	16.06	0.226	0.1624	0.0772	0.0507	5.21	3.74	2.40	
	114	0.441	0.025	0.0153	0.0164	0.0168	0.10	0.21	0.31	
V24	0.358162	16.00	0.211	0.1010	0.0573	0.0245	4.58	4.06	3.09	
(LC450)	125	0.421	0.031	0.0200	0.0193	0.0195	0.19	0.34	0.77	
V32	0.361938	16.05	0.212	0.0714	0.0845	0.0403	4.77	4.41	1.93	
(LC864)	145	0.429	0.050	0.0285	0.0290	0.0296	0.41	0.36	0.70	

Note. — LC99 discovered 13 new RR Lyrae variables in M2. In the catalog of Variable Stars in Globular Clusters at http://www.astro.utoronto.ca/people.html (Clement et al. 2001), these have been numbered V22 through V34.

Table 10. Corrected Magnitudes and Reddenings by Field

		All	Stars————————————————————————————————————			——————————————————————————————————————	ike Stars—— ——Mean——	
Field	N	$< V >_F$	E(V-R)	$< V_0 >_F$	N	$< V >_F$	E(V-R)	$< V_0 >_F$
(1)	(2)	(3)	(4)	(5)	(6)	(7)	(8)	(9)
2	32	19.25±0.03	0.06 ± 0.01	18.92±0.04	8	19.23±0.07	0.06 ± 0.02	18.91±0.08
3	22	19.50 ± 0.05	$0.13 {\pm} 0.01$	$18.84 {\pm} 0.05$	4	$19.48 {\pm} 0.05$	$0.13 {\pm} 0.02$	18.80 ± 0.05
5	34	19.25 ± 0.03	0.06 ± 0.00	18.92 ± 0.03	8	19.23 ± 0.04	0.08 ± 0.01	18.81 ± 0.05
6	36	19.36 ± 0.02	0.09 ± 0.01	18.87 ± 0.03	9	19.45 ± 0.05	0.11 ± 0.01	18.86 ± 0.07
10	14	$19.22 {\pm} 0.04$	0.06 ± 0.01	18.93 ± 0.03	6	19.23 ± 0.07	$0.05 {\pm} 0.01$	18.94 ± 0.06
11	25	19.36 ± 0.05	$0.05 {\pm} 0.01$	19.10 ± 0.06	2	$19.27 {\pm} 0.08$	$0.06 {\pm} 0.05$	18.94 ± 0.20
12	13	19.41 ± 0.04	0.09 ± 0.01	18.94 ± 0.04	2	$19.42 {\pm} 0.15$	0.10 ± 0.03	18.90 ± 0.02
13	32	19.31 ± 0.02	0.08 ± 0.01	18.91 ± 0.03	8	19.34 ± 0.05	0.08 ± 0.01	18.92 ± 0.06
14	13	19.30 ± 0.04	0.03 ± 0.01	19.15 ± 0.05	5	$19.26 {\pm} 0.05$	$0.04 {\pm} 0.01$	19.05 ± 0.07
15	13	19.56 ± 0.04	$0.11 {\pm} 0.01$	19.00 ± 0.03	3	19.62 ± 0.09	$0.11 {\pm} 0.01$	19.02 ± 0.02
18	11	$19.27 {\pm} 0.04$	$0.06 {\pm} 0.01$	18.97 ± 0.09	2	19.35 ± 0.05	$0.05 {\pm} 0.00$	19.07 ± 0.05
19	13	$19.22 {\pm} 0.04$	0.03 ± 0.01	19.05 ± 0.05	4	19.33 ± 0.03	0.03 ± 0.01	19.14 ± 0.07
47	12	$19.25 {\pm} 0.05$	$0.05 {\pm} 0.01$	18.99 ± 0.04	2	$19.28 {\pm} 0.15$	0.03 ± 0.03	19.11 ± 0.04
80	33	19.39 ± 0.04	0.13 ± 0.01	18.72 ± 0.04	10	19.43 ± 0.06	$0.12 {\pm} 0.02$	18.79 ± 0.05
81	14	$19.45 {\pm} 0.05$	$0.07 {\pm} 0.01$	19.05 ± 0.07	3	19.50 ± 0.13	0.09 ± 0.02	19.00 ± 0.23
82	13	19.37 ± 0.03	0.11 ± 0.01	18.76 ± 0.06	4	19.43 ± 0.06	0.13 ± 0.01	18.73 ± 0.11
\mathbf{ALL}	330	19.34 ± 0.01	0.08 ± 0.003	18.92 ± 0.01	80	19.35 ± 0.02	0.09 ± 0.005	18.91 ± 0.02

Note. — In each case, the errors listed represent the standard error of the mean. However, for both the extinction and V_0 , there are systematic errors as well: 0.022 mag in E(V-R), which propagates to an error of 0.12 mag in V_0

Table 11. Mean Magnitudes and Colors for the M5-like RR1 Stars in Field 80

Star (1)	$\langle V \rangle_F$ (2)	$< V>_{int}$ (3)	$\langle R \rangle_F$ (4)	$\langle R \rangle_{int}$ (5)	$\langle V \rangle_F - \langle R \rangle_F \tag{6}$	$ \langle V - R \rangle_{mag} $ $ (7) $
80.6351.2358	19.32	19.31	19.10	19.09	0.22	0.22
80.6354.3658	19.81	19.79	19.48	19.48	0.33	0.32
80.6475.3548	19.46	19.45	19.20	19.20	0.26	0.25
80.6589.2425	19.56	19.54	19.30	19.29	0.26	0.26
80.6596.3127	19.51	19.50	19.24	19.23	0.27	0.27
80.6710.2075	19.41	19.40	19.18	19.17	0.23	0.23
80.6832.2030	19.59	19.58	19.31	19.30	0.28	0.27
80.7192.4927	19.49	19.48	19.19	19.18	0.30	0.30
80.7320.1224	19.26	19.25	19.03	19.02	0.23	0.23
80.7437.1665	19.39	19.38	19.11	19.10	0.29	0.29

Table 12. Mean Magnitudes for Stars Observed by C03

	МАСНО			C03-		
ID	< V >	N_{obs}	ID	< V >	N_{obs}	$\Delta < V >$
(1)	(2)	(3)	(4)	(5)	(6)	(7)
6.6689.563*	19.22	443	2249	19.39	70	0.17^{\dagger}
13.6689.3055*	19.24	393				$0.15\dagger$
6.6812.1063	19.61	240	8837	19.58	64	-0.03
6.7054.710*	19.43	318	7864	19.48	67	0.05
13.7054.3006*	19.36	171				0.12
13.5838.667	19.39	253	7648	19.40	69	0.01
13.5959.584	19.20	423	7783	19.30	70	0.10
13.6079,604	19.25	373	4749	19.32	63	0.07
13.6201.670	19.10	462	7490	19.18	70	0.08
Mean (all)						0.07
$\mathbf{Mean} \ (\mathbf{ex} \ 2249)$						0.05

Note. — *MACHO 6.6689.563 is the same star as 13.6689.3055 and 6.7054.710 is the same star as 13.7054.3006. †C03 found excessive scatter in the light curve for their star #2249.

FIGURES

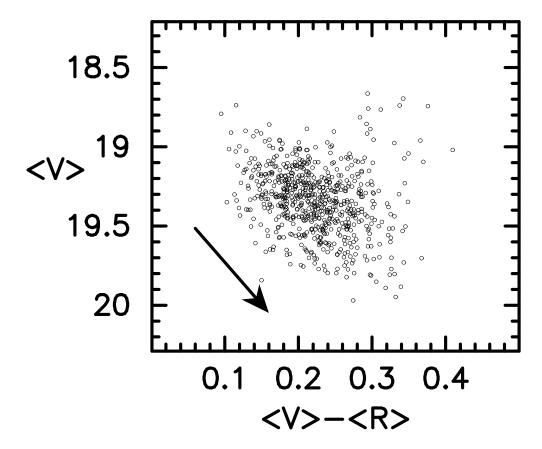


Fig. 1.— $< V>_F$ vs $< V>_F - < R>_F$ for the stars listed in Table 1. The reddening vector $(A_V/E(V-R)=5.35)$ is marked with an arrow.

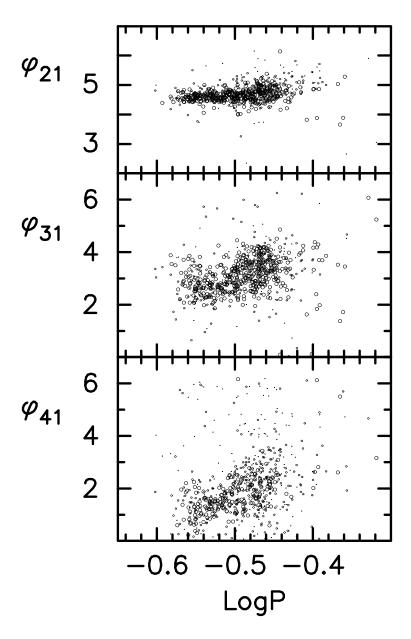


Fig. 2.— Fourier phase differences ϕ_{21} , ϕ_{31} and ϕ_{41} as a function of log P for the V data of the 663 program stars summarized in Table 8. The plotted points are open circles that have 3 sizes: the larger the size, the lower the error. For ϕ_{21} , the largest size denotes standard errors less than 0.2, the smallest size denotes errors greater than 0.4 and the intermediate size denotes errors between 0.2 and 0.4. For the ϕ_{31} and ϕ_{41} plots, the three sizes denote standard errors less than 0.4, greater than 0.8 and between 0.4 and 0.8, respectively.

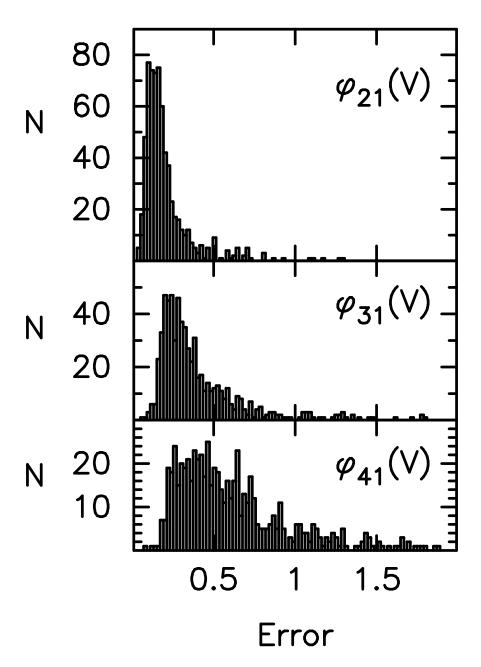


Fig. 3.— Histograms illustrating the distribution of the standard errors in ϕ_{21} , ϕ_{31} and ϕ_{41} for the V data that are plotted in Fig. 2.

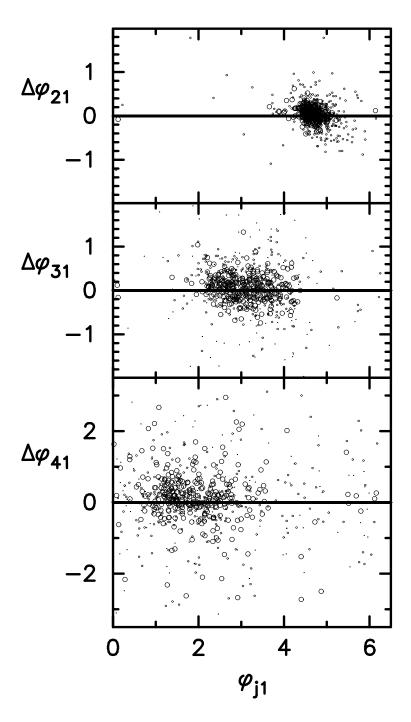


Fig. 4.— Plots of $\Delta\phi_{21}$ vs $\phi_{21}(V)$, $\Delta\phi_{31}$ vs $\phi_{31}(V)$ and $\Delta\phi_{41}$) vs $\phi_{41}(V)$, to illustrate the effect of color on the Fourier phase differences. The $\Delta\phi_{j1}$ values denote $[\phi_{j1}(R) - \phi_{j1}(V)]$. The horizontal lines are drawn at $\Delta\phi_{j1} = 0$. The scaling of the plotted points (open circles) is the same as in Fig. 2, i.e. the different sizes correspond to the errors in the Fourier coefficients for the V data.

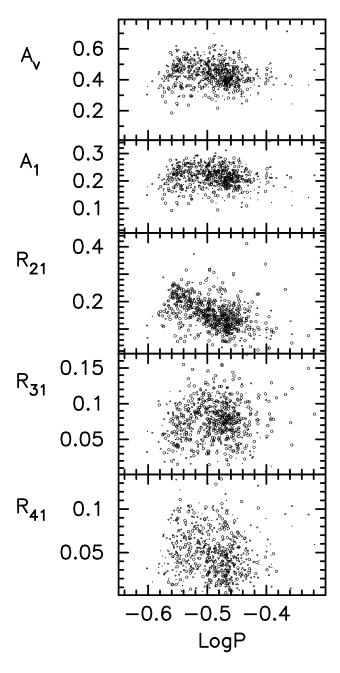


Fig. 5.— V amplitude, Fourier amplitude A_1 and amplitude ratios R_{21} , R_{31} and R_{41} for the V data as a function of $\log P$. The plotted points are open circles that have three sizes, as in Figs. 2 and 4. For A_V and A_1 , the largest size denotes stars for which the standard deviation (σ) of the fit to equation (1) is less than 0.06, the smallest size denotes σ greater than 0.08 and the intermediate size denotes σ between 0.06 and 0.08. For the R_{21} , R_{31} and R_{41} plots, the scale of the points is the same as in Fig. 2. It relates to the errors in the Fourier phase differences for the V data.

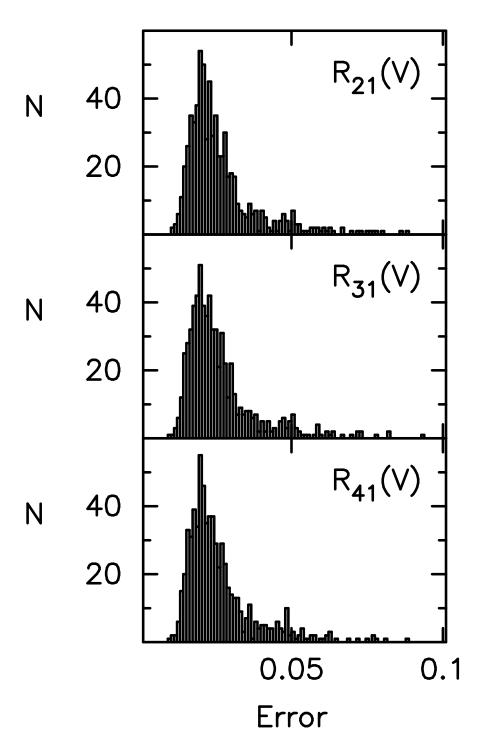


Fig. 6.— Histograms illustrating the distribution of the standard errors in R_{21} , R_{31} and R_{41} for the V data plotted in Fig. 5.

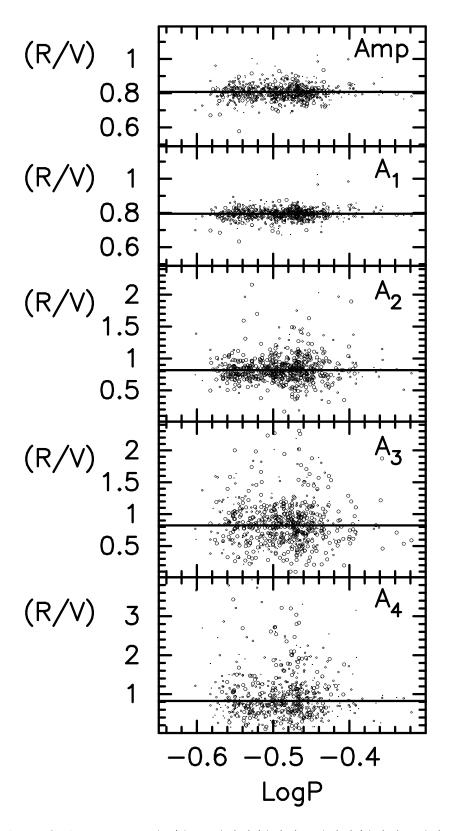


Fig. 7.— Plots of the ratios: A_R/A_V , $A_1(R)/A_1(V)$, $A_2(R)/A_2(V)$, $A_3(R)/A_3(V)$ and $A_4(R)/A_4(V)$ to show the effect of wavelength band. The symbols are the same as in Figure 5.

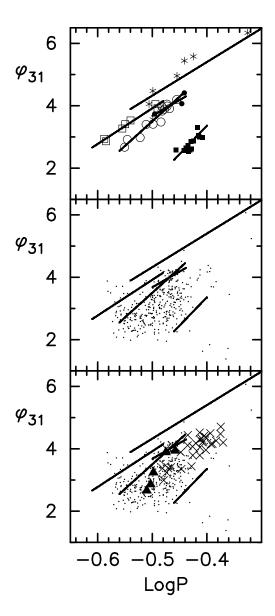


Fig. 8.— In the upper panel, we plot ϕ_{31} vs $\log P$ for the RR1 variables in five well studied Galactic globular clusters. The different symbols represent different clusters: asterisks for NGC 6441, open squares for M107 (NGC 6171), open circles for M5, solid circles for M2 and solid squares for M68. For each cluster, a straight line derived from a least squares fit is plotted through the points. In the central panel, these lines are repeated and the points for the RR1 variables in the LMC for which the error in ϕ_{31} is less than 0.4 are also plotted. The lower panel is the same as the central panel with the RR1 stars in two additional clusters, ω Centauri (crosses) and M3 (solid triangles) included.

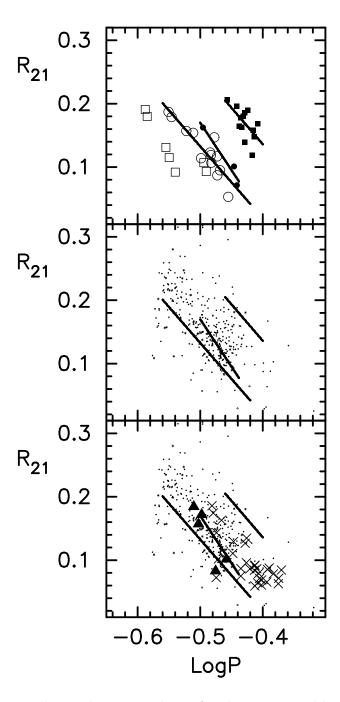


Fig. 9.— In the upper panel, we plot R_{21} vs $\log P$ for the RR1 variables in four clusters: open squares for M107 (NGC 6171), open circles for M5, solid circles for M2 and solid squares for M68. For M5, M2 and M68, a straight line derived from a least squares fit is plotted through the points. In the central panel, these lines are repeated and the points for the RR1 variables in the LMC for which the error in R_{21} is less than 0.025 are also plotted. The lower panel is the same as the central panel with the RR1 stars in two additional clusters, ω Centauri (crosses) and M3 (solid triangles) included.

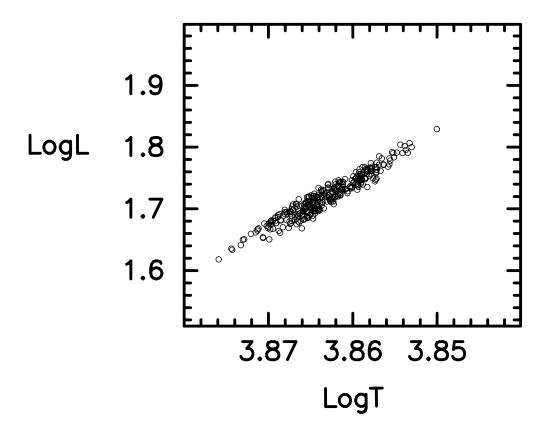


Fig. 10.— $\log L/L_{\odot}$ calculated from equation (2) versus $\log T_{eff}$ calculated from equation (5) for the V data. Only the 330 stars for which the period is in the range $-0.56 < \log P < -0.4$, $\sigma(\phi_{31}) < 0.4$, the amplitude $A_V > 0.3$ and the amplitude ratio A_R/A_V is greater than 0.75 and less than 0.85 are included. These are the stars considered to be RR1 variables and are referred to as the bona fide RR1 variables throughout the paper.

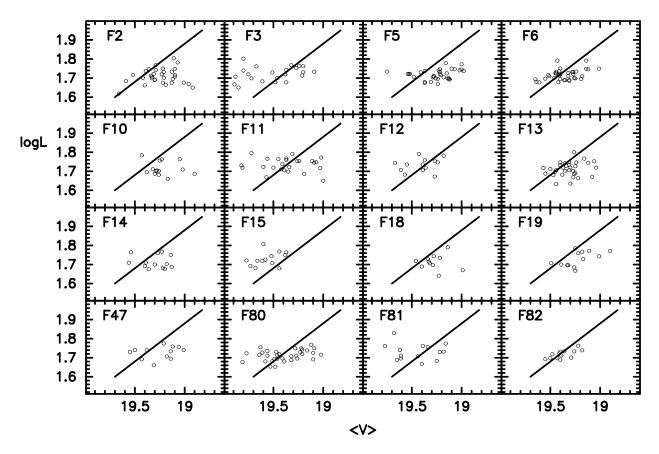


Fig. 11.— Plots of $\log L/L_{\odot}$ versus the mean V magnitude for the 330 RR1 variables plotted in Figure 10. The stars in each field are plotted separately and the line drawn through the points in each panel has a slope $\Delta \log L/\Delta V = -0.4$. The lines are plotted at the same position in each panel so that differences in < V > among the fields can be readily observed.

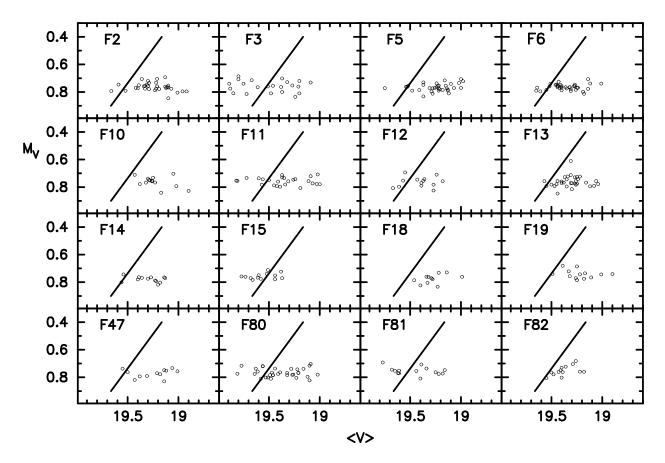


Fig. 12.— Plots of M_V calculated from equation (3) versus < V > for the 330 RR1 variables plotted in Figure 10. The stars in each field are plotted separately and the line drawn through the points in each panel has a slope $\Delta M_V/\Delta V = 1$.

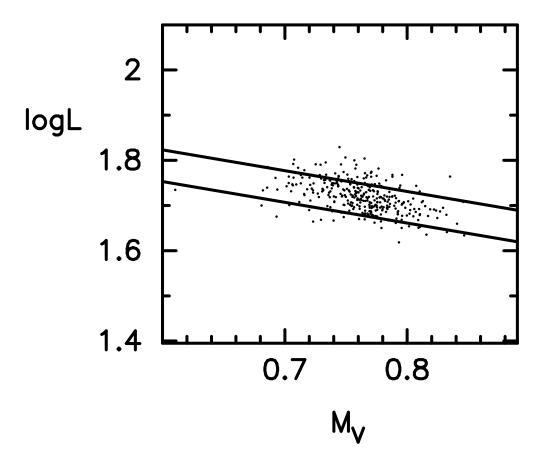


Fig. 13.— $\log L/L_{\odot}$ versus M_V calculated from equations (2) and (3) using the V data for the 330 RR1 variables plotted in Figure 10. The envelope lines have a slope of -0.46, the predicted slope for $\Delta \log L/\Delta M_V$ and are separated by $\Delta \log L = 0.07$.

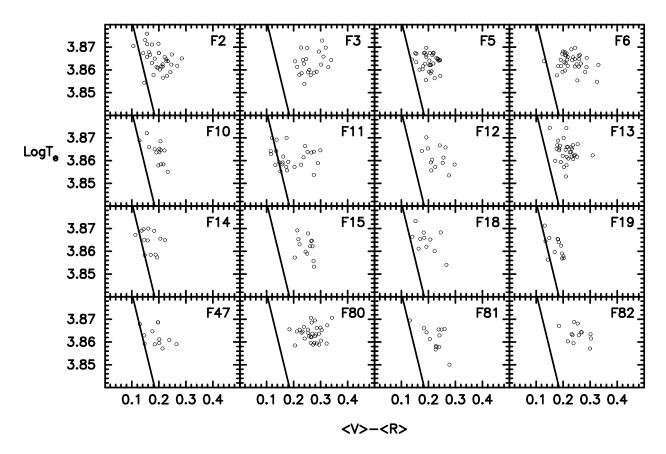


Fig. 14.— $\log T_{eff}$ versus $[< V>_F - < R>_F]$ for the 330 RR1 variables plotted in Figure 10. The stars in each field are plotted separately to show the differences in color excess. The ridge lines represent the $\log T_{eff} - (V - R)_0$ relations derived from equation (6) assuming $\log g = 2.9$ and $[\mathrm{M/H}] = -1.5$.

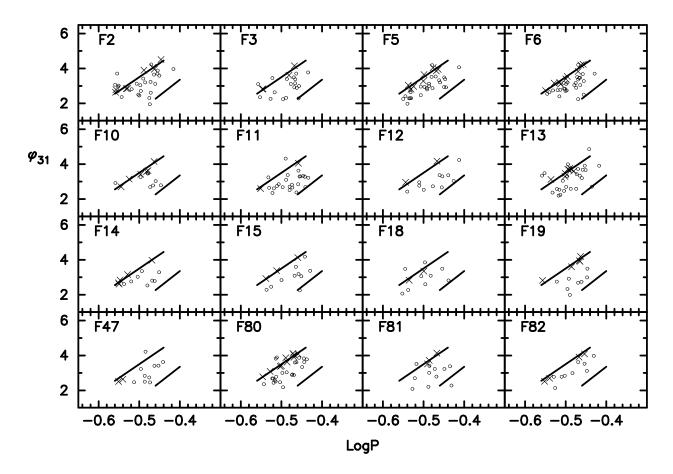


Fig. 15.— Plots of ϕ_{31} vs $\log P$ for the 330 RR1 variables plotted in Figure 10, with each field plotted separately. The straight lines are the M5 and M68 lines from Fig. 8. The 'M5-like' variables are designated as crosses.

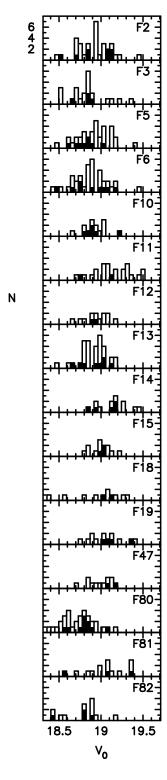


Fig. 16.— The distribution of V_0 for the 330 RR1 variables plotted in Figure 10, with each field plotted separately. The solid areas represent the 'M5-like' variables.

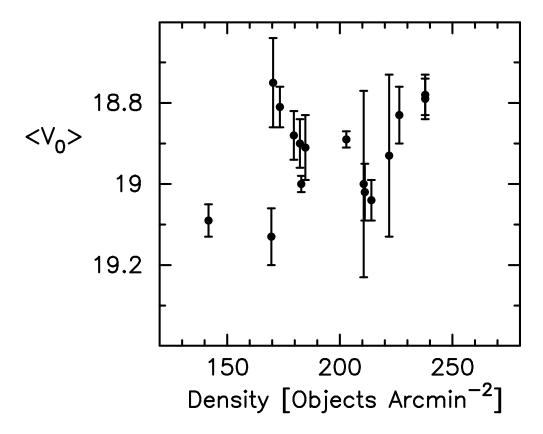


Fig. 17.— The mean V_0 for the M5-like variables versus the density for the 16 fields. The mean V_0 value for each field has been adjusted to compensate for the distance D/D_0 , listed in column (4) of Table 8 and the error bar represents the standard deviation of V_0 within the field. The density is the average number of objects per square arcmin, listed in column (5) of Table 8.